2016

Cell Capacitance Estimation and Detection

Stephen A. Sladen
University of Rhode Island, stephen_sladen@my.uri.edu

CELL CAPACITANCE ESTIMATION AND DETECTION

BY

STEPHEN A. SLADEN

A THESIS SUBMITTED IN PARTIAL FULFILLMENT OF THE

REQUIREMENTS FOR THE DEGREE OF

MASTER OF SCIENCE

IN

ELECTRICAL ENGINEERING

UNIVERSITY OF RHODE ISLAND

2016

MASTER OF SCIENCE THESIS

OF

STEPHEN A. SLADEN

APPROVED:

Thesis Committee:

Major Professor Ying Sun

Steven M. Kay

Mustafa Kulenovic

Nasser H. Zawia

DEAN OF THE GRADUATE SCHOOL

UNIVERSITY OF RHODE ISLAND

2016

ABSTRACT

The aim of this thesis is to examine the behavior of the electrical properties such as the resistance and capacitance of the cell membrane. During specific biological processes, the electrical properties of the membrane can yield useful data which can be further exploited to study these phenomenons. Using simulations, an accurate model of the cell membrane was built based on a three-element analog electrical circuit. Presented in this thesis are several signal processing algorithms which are used to either estimate the parameter values of the model or detect the presence of a vesicle activity.

The estimation is achieved with least-squares estimation using three methods, one being a nonlinear estimation problem. The two non-iterative linear estimators involve invoking the linear model to fit the data set and the use of a matched filter followed by the use of cross-correlation. The nonlinear estimator is of the separable type, however associated is an extensive run time, undesirable in a real-time setting. The detection method uses a variety of low-pass filters and a trigonometric identity to detect a change in the phase of the filtered output, a very similar method seen in lock-in amplifiers. In both sets of algorithms, sufficient cycles from the sinusoidal excitations are ensured to produce results to within 99% of the true values.

ACKNOWLEDGMENTS

I would like to thank my advisor, Dr. Ying Sun for everything he has done for the Biomedical Engineering department and continues to do so, whether it be the conferences, the Capstone projects, or even the semi-annual buffet parties. Thank you for being such a wonderful professor and allowing me to engage in the research presented in this thesis. I would like to thank Dr. Vetter for allowing me to work with him several summers ago, also for being there when I had to discuss how I got to where I am today. Thank you Dr. Kay for being one of the most inspirational professors I have ever had the honor of meeting. The coursework I engaged myself in throughout the past year under his teaching has opened a whole new world of potential. Also, Dr. Kulenovic for being an excellent mathematics professor, whose clear and concise instructions benefited my success in several of my graduate courses. Dr. Boudreaux-Bartels, thank you for introducing me to signal processing, your courses inspired me to pursue a further understanding of the field. Also, a thank you is in order for Dr. Jouaneh for taking the time this summer to serve as my committee chair. The author would also like to thank Dr. DiCecco for the Latex help in putting this thesis together, and for the many interesting chats over the years.

DEDICATION

This thesis is dedicated to the people who mean the most to me in my life: Mom, I owe you everything to you. Your countless demonstrations of selfless to ensure your children would succeed, I don't know if there is enough gratitude in the world to repay you. Ryan, my brother, always trying to help me become a better person and for always being there. Thanks Ry. I would like to thank my grandfather Anthony Landi for being a father figure over all the years, you truly are a great man, and you have always been my inspiration. I would also like to dedicate this to my grandparents Jane and Leo Sladen for for all the love and support I have received from them over all these years. For Benny, my buddy. And to all my friends, you know you are.

Last, this thesis is dedicated to my grandmother, Barbara Landi. This is for you.

PREFACE

In previous works [Sladen, Phongsavan 2013], the subject of modeling biological processes was explored through design of a *neuron emulator*, capable of modeling an neuronal action potential. By using a microprocessor (PIC18F4525, Microchip Technology, Chandler, AZ) as the main controlling component and analog circuit components, action potentials were generated using a voltage-controlled switch (MC14016). The motivation for the experiment was to design a device capable of being testing by the device known as the Universal Clamp (UC), an instrument capable of a variety of clamp techniques involving a single-electrode setting.

In a separate experiment performed by other students [Cullen, Patel, Shannon 2014], a hardware implementation of a three-element model was constructed to study cellular capacitance. By using the PIC18F4525 to generate a switching sinusoidal excitation, it was possible to time-multiplex the voltage with the current measurements on a single-electrode setting, made possible by [Neher, Bakmann]. The signal was then modulated via a transistor (MOSFET) and injected into the model to induce a response that contained the phase shift associated with vesicle activity.

This work was inherited by [Rosenberg, Hammick 2016] where the aims of the project was to simulate and record the small capacitance changes on the order of (100×10^{-15}) Farads that could not be achieved with the previous design. Using the PIC18F4525, pulses of a specified duty cycle and frequency were generated and sent through branches of capacitors in order to monitor the small differences between capacitors of "equal" value. The term "equal" refers to the ($\pm 10\%$) error tolerance in the nominal values. By using a precise capacitance meter (Model 3000 GLK Instruments, San Diego, CA), a capacitance change of 20 pF corresponds with

a voltage output of 200 mV. Although the accuracy of the capacitance meter is on the order 1 fF at a time resolution of 1 ms, the capability of the analog-to-digital converter (ADC) (USB-1208FS, Measurement Computing, Norton, MA) could not achieve such a resolution due to the sampling rate.

For this thesis, the future works of [Cullen, Rosenberg] involving the design of signal processing algorithms for parameter estimation and phase detection are investigated.

This study was supported in part by a grant from the National Institute of Health (1R43NS087659-01A1, PI: Sun).

TABLE OF CONTENTS

LIST OF FIGURES

CHAPTER 1

Introduction

1.1 Background

The motivation for this thesis work stems from the need for a means to monitor the cell capacitance accurately and continuously. The phospholipid bilayer, which is the basic structure of the cell membrane is made up of an arrangement of phospholipids such that the hydrophilic heads face the cytosol inside the cell, while the hydrophobic tails face each other extracellular fluid (ECF) outside the cell. The membrane itself appears electrically as a thin insulator which separates two electrolytic regions, therefore it may be appropiately modeled as a capacitor [1]. Typically the *total* membrane capacitance is fairly constant in proportion to the surface area of the membrane ($0.5 - 1.0\ \mu F/cm^2$) [2, 3] or simply larger membrane area, larger capacitance. For the membrane resistance, the smaller the membrane area, the larger the resistance of the membrane.

By monitoring the cell in a real-time setting, it can be shown that during active transport processes that these two quantities changes momentarily. The type of processes referred to are ones in which macromolecules are too large to cross the membrane, even with the assistance of proteins [4]. Thus, the molecules are facilitated across via the formation of vesicles called endosomes. During the intake process called endocytosis, the molecules in the ECF enter the cell through the endosomes from the membrane. The "reverse" process, exocytosis, involves packaging the molecules into secretory vesicles which fuse with the membrane, eventually releasing the contents back into the ECF. For this research, simulations using signal processing algorithms have been implemented using MATLAB on an accurate electrical model in order to estimate the value of the membrane capacitance or to detect whether or not the vesicle activity referred to is in fact

occurring.

1.2 Signal Acquisition

A typical electrical model of the cell membrane consists of a resistor R_m placed in parallel with a capacitor C_m with a time constant $\tau = R_m C_m$. Although it has been shown in literature [5] that the true membrane resistance is on the order of giga-ohms, the component values in this experiment were chosen to be a 10 MΩ and 5 pF respectively due to the availability of hardware. The electrode used to access the cell is represented as a 1 MΩ resistor R_a for which is placed in series with the cell membrane model. It is a nearly universal assumption that $R_m \gg R_a$. The complete 3-element model is shown in Fig. 1. To examine the behavior of

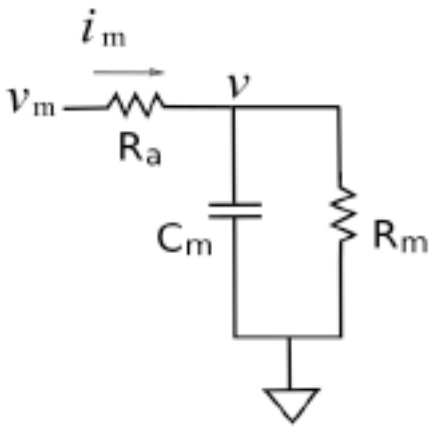

Figure 1. The 3-element model of the cell membrane with access electrode.

this model, linear circuit techniques (i.e. Laplace Transforms) are applied to Fig. 1 to determine the admittance function for which is known to be a function of frequency [5]. In order to do so, first each component must be expressed in terms of its impedance, therefore we will let $Z_{R_a} = R_a$, $Z_{R_m} = R_m$, and $Z_{C_m} = \frac{1}{sC_m}$. By first only considering the membrane model, we take the equivalent parallel

impedance by taking the product over the sum of the two, given by

$$\frac{R_m \frac{1}{sC_m}}{R_m + \frac{1}{sC_m}} = \frac{R_m}{1 + sR_mC_m} \tag{1}$$

To incorporate the series resistor into the complete model we simply add it to (1) to gives us

$$\frac{R_m + R_a + sR_aR_mC_m}{1 + sR_mC_m} \tag{2}$$

Now letting $R_t = R_a + R_m$ and let $R_p = \frac{R_aR_m}{R_t}$ and reciprocating (2) so that we can determine the admittance function since the two have an inverse relationship, we have

$$\frac{1 + sR_mC_m}{R_t + sR_pR_tC_m} \tag{3}$$

by taking the complex conjugate of (3) we are able to separate this complex function into its real and imaginary parts.

$$\frac{R_t(1 + w^2R_mR_pC_m^2)}{R_t^2 + w^2R_p^2C_m^2} + j\frac{w(R_tR_mC_m - R_tR_pC_m)}{R_t^2 + w^2R_p^2C_m^2} \tag{4}$$

Factoring to eliminate terms, we have

$$\frac{1 + w^2R_mR_pC_m^2}{R_t(1 + w^2R_p^2C_m^2)} + j\frac{wC_m(R_tR_m - R_tR_p)}{R_t^2(1 + w^2R_p^2C_m^2)}$$

which leads us to our final expression for the admittance function of the system

$$Y(j\omega) = \frac{1 + w^2R_mR_pC_m^2}{R_t(1 + w^2R_p^2C_m^2)} + j\frac{wR_m^2C_m}{R_t^2(1 + w^2R_p^2C_m^2)}. \tag{5}$$

Although (5) assumes that the three variables of the model are unknowns, to avoid the nonlinearity of the admittance function, a two-step process involves recording the resistance of the access electrode prior to probing the cell membrane, thus eliminating the unknown variable R_a. In a whole-cell experiment, most often the Johnson noise associated with the Mega-Ohm resistors in the hardware limits the resolution of the capacitance measurement at high frequencies [6].

Now that a transfer function for the system has been obtained, next we describe the input. For this experiment, a single-frequency sinusoidal current, shown in Fig. 2, is injected into the model, the input given as

$$i_m = I_m sin(\omega t) \tag{6}$$

where I_m is the magnitude of the current, chosen to be 500 nA, $\omega = 2\pi f$ is the

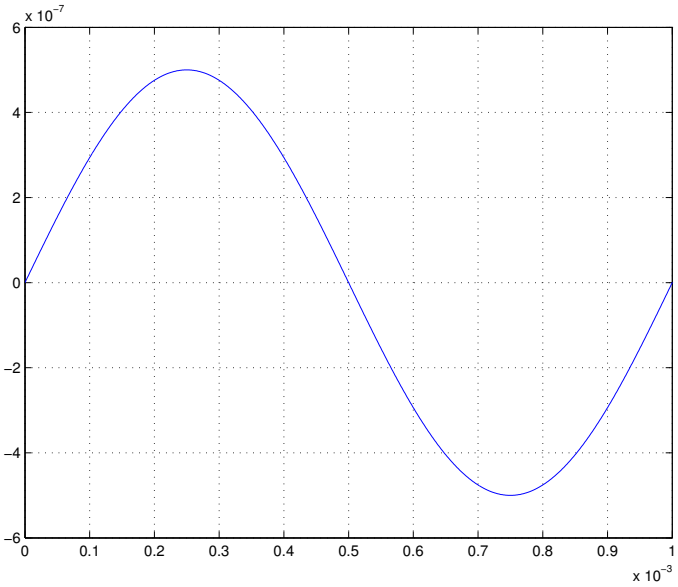

Figure 2. The injection current.

angular frequency (rads/sec), and the input frequency f is chosen to be 1 KHz. Current is injected for a time record of 1 second at a sampling frequency f_s of 1 MHz, producing a million samples, which is sufficient for this estimation problem, due to the magnitude of C_m.

Choosing the input frequency is not an arbitrary choice however, recall that impedance which is a function of frequency can be written as

$$impedance = conductance + j * susceptance$$

Capacitance measurements using lock-in amplifiers (LIAs) have been seen to be sensitive to large conductance changes. Therefore an "optimal" excitation fre-

quency would be one that obtains a small conductance-to-susceptance ratio, clearly making this quantity circuit parameter dependent [1].

Now that we have an input and a transfer function that characterizes the system, an sinusoidal output of the same frequency can be determined. The magnitude and phase of (5) can be respectively found using

$$|Y(j\omega)| = \frac{1}{\sqrt{Real(Y(j\omega))^2 + Imag(Y(j\omega))^2}} \tag{7}$$

and

$$\angle Y(j\omega) = \arctan \frac{Imag(Y(j\omega))}{Real(Y(j\omega))} \tag{8}$$

Using (7) and (8), the magnitude V_m and the phase ϕ of the input voltage v_m can now be determined.

$$V_m = I_m * |Y(j\omega)|$$

$$\phi = 0 - \angle Y(j\omega)$$

Therefore, it follows that the input voltage is given by

$$v_m = V_m sin(\omega t + \phi) \tag{9}$$

However it is known that the measured input voltage, shown in Fig. 3, is contaminated with noise for which the probability density function (PDF) is unknown., for now we will assume the noise is Gaussian.

Since one of the interests at hand is detecting vesicle activity, one could also consider increasing the capacitance for a fixed time duration. That way, the cell capacitance can be measured continuously to determine if activity is present or not. Reports suggest that small changes in (5) changes the phase angle, an indicator for vesicle fusion. Therefore, for 200 milliseconds, which is the amount of time it normally takes for transport to occur, a pulse ΔC equal to 0.5 pF was added to C_m, seen in Fig. 4. Note that if a switching excitation is applied to the model, the phase

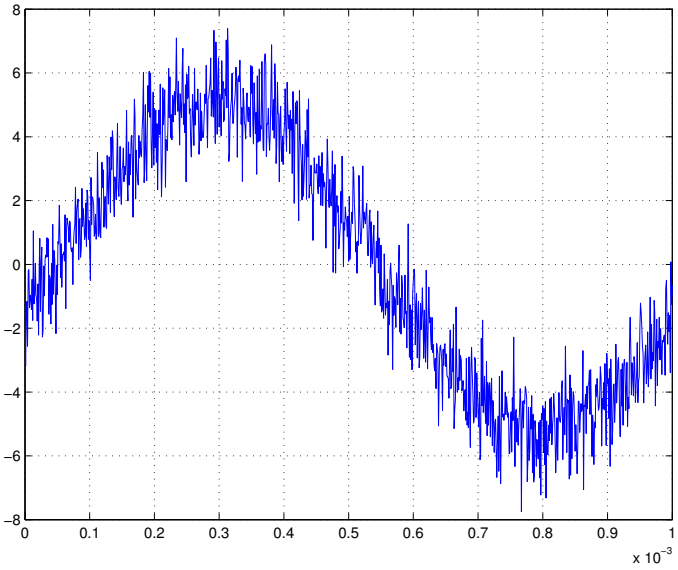

Figure 3. The induced voltage.

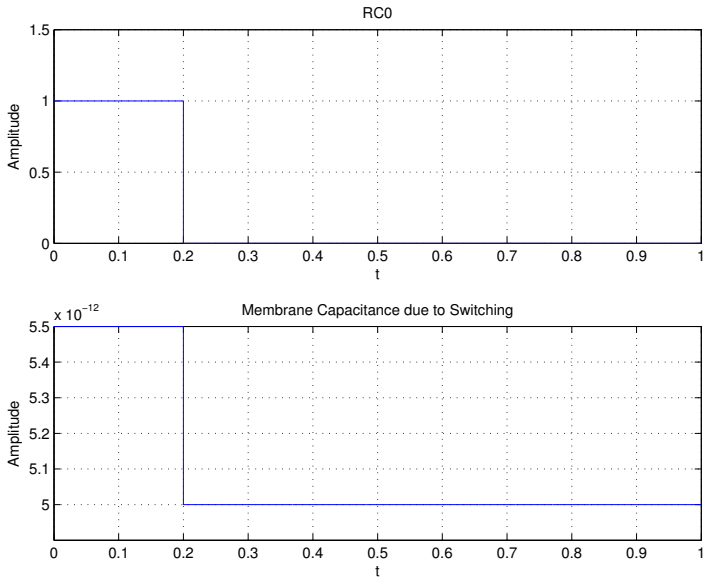

Figure 4. Switching excitation.

of the induced voltage ϕ will change as a result of the admittance function which is a time-varying function. This additional step is not required for the estimation of the unknown parameters, it simply adds more authenticity to the simulation.

List of References

[1] R. E. Thompson, M. Lindau, and W. W. Webb, "Robust, high-resolution, whole cell patch-clamp capacitance measurements using square wave stimulation," *Biophysical Journal*, vol. 81, pp. 937–948, August 2001.

[2] C. Solsona, B. Innocenti, and J. M. Fernandez, "Regulation of exocytotic fusion by cell inflation," *Biophysical Journal*, vol. 74, pp. 1061–1073, February 1998.

[3] J. Golowasch, G. Thomas, A. L. Taylor, A. Patel, A. Pineda, C. Khalil, and F. Nadim, "Membrane capacitance measurements revisited: Dependence of capacitance value on measurement method in nonisopotential neurons," *Journal of Neurophysiology*, no. 102, pp. 2161–2175, July 2009.

[4] C. L. Stanfield, *Principles of Human Physiology, 4th. edn.* San Francisco, California, United States of America: Benjamin Cummings, 2011.

[5] D. W. Barnett and S. Misler, "An optimized approach to membrane capacitance estimation using dual-frequency excitation," *Biophysical Journal*, vol. 72, pp. 1641–1658, April 1997.

[6] P. Chen and K. D. Gillis, "The noise of membrane capacitance measurements in the whole-cell recording configuration," *Biophysical Journal*, vol. 79, pp. 2162–2170, October 2000.

CHAPTER 2

Review of Literature

In the early 1950's two biophysicists by the names of Alan Hodgkin and Andrew Huxley wrote a series of five papers that forever changed how we examine the movement of ions in a cell during an action potential. A decade later, they would later receive the Nobel Prize in Medicine for their monumental papers which essentially governed the laws of how these physiological events occur. In their fifth paper [1], they describe how the squid giant axon can be modeled using analog circuit components. Since then, it has been a well investigated subject to study the current and voltage (I/V) properties of the cell membrane during patch-clamp recordings. In recent years, during observation, additional information such as the resistance and capacitance of the membrane can be obtained. One of the most common techniques for capacitance measurements is by using a lock-in amplifier (LIA) which improves the signal-to-noise ratio (SNR) of the recorded signals which are most often embedded in noise; also due to its fast temporal resolution performance [2]. The basic principle behind a LIA is what is referred to as phase-sensitive (PS) detection, which involves an input sinusoidal excitation at a specified frequency and phase for which the amplifier uses a phase-locked-loop to generate a reference signal of the same frequency and phase. The two signals are then multiplied together and then sent through an appropriate low-pass filter (LPF) which removes the AC signal leaving a constant DC component. In essence, the PS detector acts like a narrow bandpass filter for which is it possible to discard the high frequency information [3]. For any fluctuations to occur would signify any frequency or phase shifts, however we know that the input and output frequencies of the sine waves should remain the same since the system itself is linear time-invariant

(LTI). However, since a typical LIA requires two channels, it does not lend itself to a single-electrode setting where this project attempts to combine the two concepts.

Nearly 30 years later, another monumental paper was published by Neher and Marty showed how biophysicists can study fundamental cellular processes by monitoring the cell membrane capacitance, showing how the two quantities are proprtional to one another [4]. Although they were successful in observing the capacitance change associated with the fusion of a single vesicle, the phase detection method is prone to errors due to a constantly changing system [5] due to impedance changes during a recording [2].

One paper that interested me in particular, in [6], the authors describe a dual-frequency method which used a nonlinear weighted least-squares (NWLS) to estimate the circuit parameters of the 3-element model for which they showed the NWLS method produced better estimates than that of previous dual-frequency studies by obtaining an estimator that had a variance that was 10% higher than that of the theoretical Cramér-Rao Lower Bound (CRLB). The CRLB is known to be the lowest bound possible that the variance of any *unbiased* estimator may obtain. By unbiased, that is

$$E(\hat{\theta}) = \theta \quad for\ all\ \theta$$

However, the problem of the nonlinear parameter in the admittance function was overcome using a Gauss-Newton method which is although does minimize the objective function $J(\theta)$, is an iterative method, which as seen in other iterative methods such as Newton-Raphson or a method of scoring, the algorithm may not converge [7]. Another limitation of using one of these methods involve a starting point or a "*good*" guess of what the true value should be, this is very important and should be emphasized.

In conclusion, many of the methods used in literature involve using either PS

detector analysis which relies on the admittance function which is then used to fit a LS criterion; multiple frequency inputs which yield poorer estimates than that of a single-frequency input; or complex nonlinear estimation methods. Even though all of these methods yield some pretty good results, are not suitable for a real-time application since for some methods, the model may contain some nonlinear equations for which when simulated can result in long computational times and low resolution.

List of References

[1] A. L. Hodgkin and A. F. Huxley, "A quantitative description of membrane current and its application to conduction and excitation in nerve," *Journal of Physiology*, no. 117, pp. 500–544, March 1952.

[2] N. Fidler and J. M. Fernandez, "Phase tracking: an improved phase detection technique for cell membrane capacitance measurements," *Biophysical Journal*, vol. 56, pp. 1153–1162, December 1989.

[3] Stanford Reseach Systems. "About lock-in amplifiers." 2015.

[4] E. Neher and A. Marty, "Discrete changes of cell membrane capacitance observed under conditions of enhanced secretion in bovine adrenal chromaffin cells," in *Proceedings of the National Academy of Sciences*, vol. 79, November 1982, pp. 6712–6716.

[5] C. Joshi and J. M. Fernandez, "Capacitance measurements: An analysis of the phase detector technique used to study exocytosis and endocytosis," *Biophysical Journal*, vol. 53, pp. 885–892, June 1988.

[6] D. W. Barnett and S. Misler, "An optimized approach to membrane capacitance estimation using dual-frequency excitation," *Biophysical Journal*, vol. 72, pp. 1641–1658, April 1997.

[7] S. M. Kay, *Fundamentals of Statistical Signal Processing: Estimation Theory*. Upper Saddle River, New Jersey, United States of America: Prentice Hall, 1993.

CHAPTER 3

Least-Squares Estimation

3.1 Linear Least-Squares

Consider the overdetermined equation

$$H\theta = \mathbf{s} \tag{10}$$

where H is the $m \times n$ plant matrix, θ the $n \times 1$ unknown vector, and $\mathbf{s}$ the $m \times 1$ measurement vector, where $m > n$ and no solution for $\mathbf{s}$ exists. The best thing one could do is find a solution for which the distance between the two vectors $\mathbf{s}$ and $H\theta$ is minimized. In other words, in order to find an accurate θ, the least-squares (LS) error must be minimized, given by

$$(s - H\theta)^T(s - H\theta)$$

where by following the procedure presented in Appendix A, the best approximation or estimator is given as

$$\hat{\theta} = (H^T H)^{-1} H^T s$$

In this section we present a linear least-squares estimator (LSE) to determine the an unknown vector of parameters. Since the induced voltage v_m is contaminated with noise, most likely introduced by the noise of the resistors [1], two methods are presented for which obtain an estimate of the voltage to within $\approx 99\%$ of the true signal.

A note to the reader, in the section described by using the linear model (LM), there exists two plant matrices. The first matrix H is used to estimate the amplitude and phase parameters of the waveform v_m. The second matrix A is used as the LS solution to estimate the R_m and C_m parameters.

3.1.1 Linear Model

In order to estimate the values of the membranes resistance and capacitance, we first have to estimate the values of the magnitude and phase of the input voltage. The received waveform in MATLAB is given as

$$x[n] = V_m sin(\omega n + \phi) + w[n]$$

where w[n] is the noise process associated with the received data. Using trigonometric identities, this can be rewritten as

$$x[n] = V_m cos(\phi) sin(\omega n) + V_m sin(\phi) cos(\omega n) + w[n]$$

$$= \alpha_1 sin(\omega n) + \alpha_2 cos(\omega n) + w[n]$$

where $\alpha_1 = V_m cos(\phi)$ and $\alpha_2 = V_m sin(\phi)$. It follows that then the inverse transformations are given by

$$V_m = \sqrt{\alpha_1^2 + \alpha_2^2} \tag{11}$$

$$\phi = \arctan(\frac{-\alpha_2}{\alpha_1}) \tag{12}$$

Using this transformation, the input signal can be expressed using the general linear model [2]. Using matrix notation, the signal x can be written as

$$x = H\alpha + w$$

where the $N \times 1$ vectors are given as

$$\mathbf{x} = [x[0], x[1], ..., x[N-1]]^T$$

$$\mathbf{w} = [w[0], w[1], ..., w[N-1]]^T$$

The observation matrix H is a $N \times p$ matrix where $p = 2$ and is known to be, defined as

$$\mathbf{H} = \begin{bmatrix} 0 & 1 \\ sin(\omega) & cos(\omega) \\ \vdots & \vdots \\ sin(\omega(N-1)) & cos(\omega(N-1)) \end{bmatrix}$$

Lastly, the unknown vector α for which we wish to estimate is a $p \times 1$ vector, defined as

$$\alpha = [V_m cos(\phi) \quad V_m sin(\phi)]^T.$$

The observation matrix H must obey a certain criterion in order for the linear model to be used correctly [3]. The first condition that has to be satisfied is that the matrix $H^T H$ must be invertible. The second condition is that the columns of H are linearly independent (i.e. H is of rank p, where $N > p$).

Note that we have not discussed the noise vector w. This is due to the fact that we have not made any probabilistic assumptions about it, only having knowledge of the signal model. This leads us to the use of a least-squares estimator (LSE) to estimate the unknown vector α. It can be shown in [2] that although no optimality exists for this type of estimator, when the noise samples are in fact zero-mean white Gaussian where each sample is independent and identically distributed (IID) that the LSE is in fact equivalent to what is known as the *maximum likelihood estimator*, which is the most commonly estimator in practice due the ease of its implementation. When applying the linear model, we will just assume that the noise process is white Gaussian noise (WGN), which is characterized as $w \sim N(0, \sigma^2)$, where $\sigma^2 = 1$, however this model is used for other general noise PDFs [2, 4].

Since the conditions of the linear model have been satisfied, the LSE is given as

$$\hat{\alpha} = (H^T H)^{-1} H^T x \tag{13}$$

where

$$\hat{\alpha} = \begin{bmatrix} \widehat{\alpha_1} \\ \widehat{\alpha_2} \end{bmatrix} = \begin{bmatrix} \widehat{V_m} cos\hat{\phi} \\ \widehat{V_m} sin\hat{\phi} \end{bmatrix}$$

Using (11)and (12) the estimates for V_m and ϕ can be found by

$$\widehat{V_m} = \sqrt{\widehat{\alpha_1}^2 + \widehat{\alpha_2}^2} \tag{14}$$

$$\hat{\phi} = \arctan(\frac{-\widehat{\alpha_2}}{\widehat{\alpha_1}}) \tag{15}$$

Once (14) and (15) have been determined, an estimate for the input voltage $\widehat{V_m}$ can be determined to be

$$\widehat{v_m} = \widehat{V_m} sin(\omega t + \hat{\phi}) \tag{16}$$

for which will be one of the signals used in the plant matrix used to estimate R_m and C_m.

3.1.2 Correlation Method

An alternative approach of extracting the amplitude V_m and phase ϕ from the noisy data $x[n]$ is by correlating the data with a replica of the known deterministic signal $s[n]$. More specifically, this is done by relating the correlation to the effect of a finite impulse response (FIR) filter on the data [5]. The filter works by using the data $x[n]$ as the input and convolves it with an impulse response h[n] that is a "flipped around" version of the known signal model, that is,

$$h[n] = s[N-1-n] \quad for \quad n = 0, 1, ..., N-1$$

Then the output of the filter $y[n]$ is given by the convolution sum

$$y[n] = \sum_{k=0}^{n} h[n-k]x[k] = \sum_{k=0}^{n} s[N-1-(n-k)]x[k] \tag{17}$$

For the output at the last sample $n = N-1$

$$y[N-1] = \sum_{k=0}^{N-1} s[k]x[k] \tag{18}$$

which with a change of variables is identical to that of the Neyman-Pearson detector (See [5], pages 95-96), also known as a *matched filter* (MF). Therefore, we let the impulse response $h[n]$ be the flipped version of the known signal $s[n] = v_m[n]$, then the MF is

$$y[n] = \sum_{k=0}^{n} v_m[n-k]x[k]$$

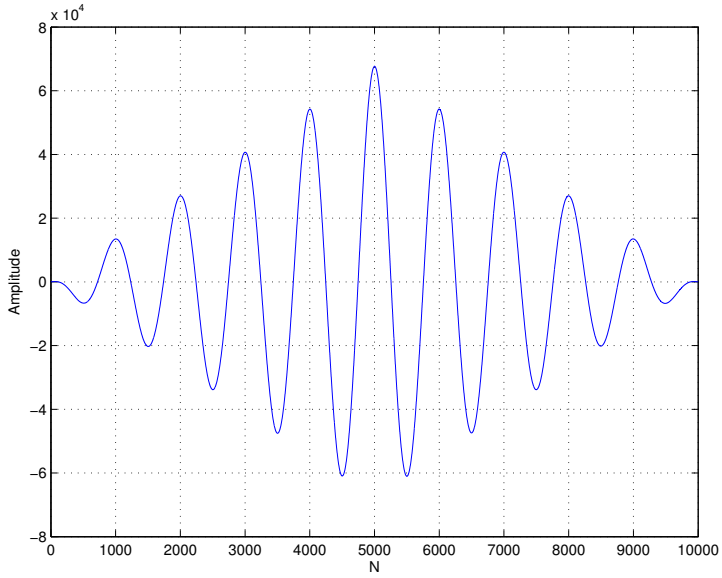

Figure 5. The output of the Matched Filter.

which the output of can be seen in Fig. 5.

Once the output of the filter y[n] has been obtained, the amplitude of the unknown $v_m[n]$ can be found by

$$\widehat{V_m} = \sqrt{\frac{2y_{max}[n]}{T}} \tag{19}$$

where T is a chosen number of samples to guarantee a full cycle of the sine wave. For this simulation it was chosen that five cycles (T = 5000 samples) was sufficient for this problem. However it was seen that a different number of cycles slightly changed the estimated values but this is expected since we are using more data in the estimation algorithms which in turn tends to yield better results.

An estimate for the phase ϕ is found using a method involving cross-correlation (CC). Since we are dealing with discrete signals in MATLAB, the cross-correlation sequence (CCS) is given as

$$r_{X,Y}[k] = E[X[n]Y[n+k]] \quad for \quad k = ..., -1, 0, 1, ... \tag{20}$$

where $X[n]$ and $Y[n]$ are assumed to be *individually* wide-sense stationary (WSS),

then the CCS $r_{X,Y}[k]$ is said to be *jointly* WSS [6]. From this, three important properties follow:

Property 1: The CCS is not necessarily symmetric:

$$r_{X,Y}[-k] \neq r_{X,Y}[k]$$

Property 2: The maximum of the CCS can occur for any value of k.

Property 3: Interchanging $X[n]$ and $Y[n]$ flips the CCS about $k = 0$:

$$r_{X,Y}[-k] = r_{Y,X}[k]$$

By letting $X[n] = i_m[n]$ and $Y[n] = v_m[n]$, we apply (20) using T samples. Then the estimate for the phase $\hat{\phi}$ is found by

$$\hat{\phi} = \frac{2\pi R_{max}}{f} \tag{21}$$

where R_{max} is the sample of the CCS for which its maximum is achieved. The output of the cross-correlation is shown in Fig. 6 where each of the three properties can be observed.

As we did in the previous section, now an estimate for the input voltage $\widehat{v_m}$ can be given as

$$\widehat{v_m} = \widehat{V_m} sin(\omega t + \hat{\phi}) \tag{22}$$

for which can be used in the LSE to determine the unknowns R_m and C_m.

3.1.3 Linear Least-Squares Algorithm

Since this was performed via simulation, prior to the additive WGN, the true values for the amplitude and phase for the input voltage was known to be

$$V_m = 5.2009$$

$$\phi = -0.3013$$

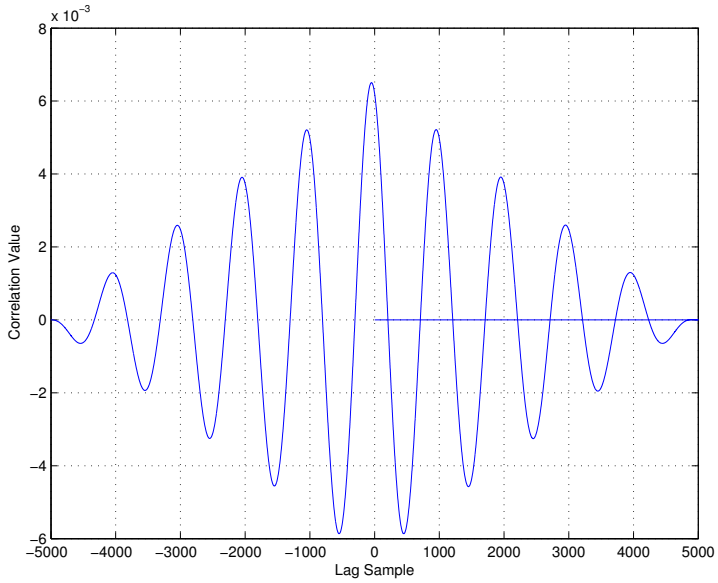

Figure 6. The cross-correlation output $r_{X,Y}[k]$.

From the linear model, the estimates were found to be

$$\widehat{V_m} = 5.2067$$

$$\hat{\phi} = -0.3060$$

Using these results, a sufficient estimate for v_m has now been found. This in addition to having knowledge of the input current i_m, the plant matrix $\mathbf{A}$ can be constructed. A comparison between the true v_m and the estimate $\widehat{v_m}$ using the linear model can be seen in Fig. 7, while the true versus the estimate using the MF/CC method shown in Fig. 8. Using this matrix $\mathbf{A}$, next we must define and derive the *derivative* variable x. Recall that the input current i_m was defined as

$$i_m = I_m sin(\omega t) \tag{23}$$

and the input voltage was determined to be

$$v_m = V_m sin(\omega t + \phi). \tag{24}$$

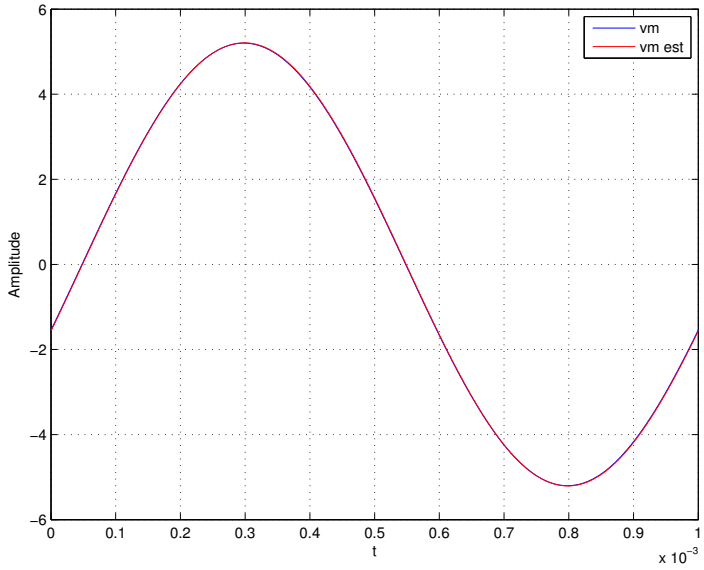

Figure 7. The true input voltage versus an estimate of the input voltage using the linear model.

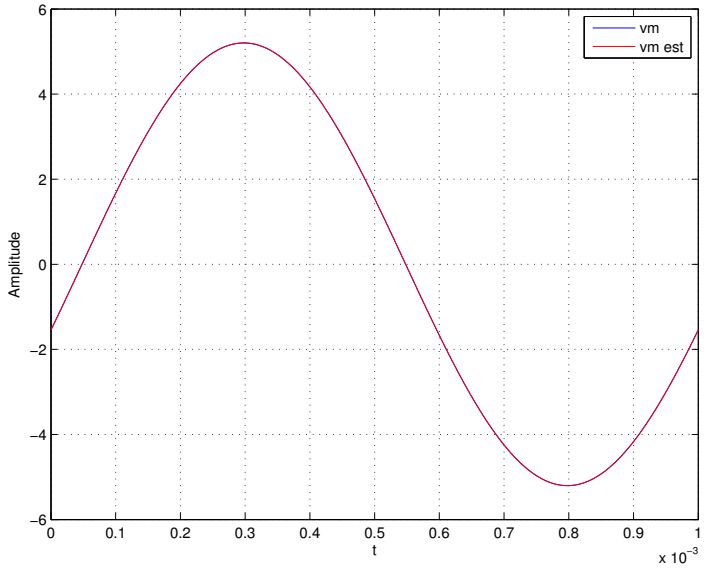

Figure 8. The true input voltage versus an estimate of the input voltage using correlation.

Applying Kirchoff's current law (KCL) to the 3-element model,

$$i_m = C_m \frac{dV}{dt} + \frac{V}{R_m} = \frac{v_m - v}{R_a} \tag{25}$$

From (25)

$$v = v_m - R_a i_m \tag{26}$$

$$v' = v'_m - R_a i'_m \tag{27}$$

Substituting (26) and (27) into (25), we have

$$i_m = C_m(v'_m - R_a i'_m) + \frac{1}{R_m}(v_m - R_a i_m) \tag{28}$$

Rearranging the terms in (28)

$$C_m(v'_m - R_a i'_m) = (1 + \frac{R_a}{R_m})i_m - \frac{1}{R_m}v_m$$

$$v'_m - R_a i'_m = (\frac{1}{C_m} + \frac{R_a}{R_m C_m})i_m - \frac{1}{R_m C_m}v_m \tag{29}$$

Next, we define the derivative variable to be

$$x = v'_m - R_a i'_m \tag{30}$$

which can be expressed as

$$x = i_m\theta_1 + v_m\theta_2 \tag{31}$$

where

$$\theta = \begin{bmatrix}\theta_1 \\ \theta_2\end{bmatrix} = \begin{bmatrix}\frac{1}{C_m} + \frac{R_a}{R_m C_m} \\ -\frac{1}{R_m C_m}\end{bmatrix}$$

By taking the derivatives of (23) and (24)with respect to ω we have

$$i'_m = \omega I_m cos(\omega t) \tag{32}$$

$$v'_m = \omega V_m cos(\omega t + \phi) \tag{33}$$

Substituting (32) and (33) into (30) produces

$$x = \omega V_m cos(\omega t + \phi) - \omega R_a I_m cos(\omega t). \tag{34}$$

Note that x can now be fit the linear model

$$x = A\theta + w$$

$$x = \begin{bmatrix} \omega V_m cos(\omega t_1 + \phi) - \omega R_a I_m cos(\omega t_1) \\ \omega V_m cos(\omega t_2 + \phi) - \omega R_a I_m cos(\omega t_2) \\ \vdots \\ \omega V_m cos(\omega t_N + \phi) - \omega R_a I_m cos(\omega t_N) \end{bmatrix}$$

where

$$A = \begin{bmatrix} i_{m1} & v_{m1} \\ i_{m2} & v_{m2} \\ \vdots & \vdots \\ i_{mN} & v_{mN} \end{bmatrix}$$

and θ was defined above. Since the conditions for the linear model have been met and no assumptions have been about the noise PDF, the LSE for θ is given by

$$\hat{\theta} = (A^T A)^{-1} A^T x \tag{35}$$

for which can be used to generate estimates for $\widehat{R_m}$ and $\widehat{C_m}$. It follows then the estimate for θ is given as

$$\hat{\theta} = \begin{bmatrix} \widehat{\theta_1} \\ \widehat{\theta_2} \end{bmatrix} = \begin{bmatrix} \frac{1}{\widehat{C_m}} + \frac{R_a}{\widehat{R_m C_m}} \\ \frac{-1}{\widehat{R_m C_m}} \end{bmatrix} \tag{36}$$

Then solving for $\widehat{C_m}$ from (36)

$$\widehat{C_m} = \frac{-1}{\widehat{R_m}\widehat{\theta_2}} \tag{37}$$

Substituting (37) into $\widehat{\theta_1}$

$$\widehat{\theta_1} = -\widehat{R_m}\widehat{\theta_2} + \frac{R_a}{\widehat{R_m}}(-\widehat{R_m}\widehat{\theta_2})$$

$$\widehat{\theta_1} = -(\widehat{R_m} + R_a)\widehat{\theta_2} \tag{38}$$

Solving for $\widehat{R_m}$

$$\widehat{R_m} = -(\frac{\widehat{\theta_1}}{\widehat{\theta_2}} + R_a) \tag{39}$$

By substituting (39) into (37), $\widehat{C_m}$ can now be determined

$$\widehat{C_m} = \frac{1}{\widehat{\theta_1} + R_a\widehat{\theta_2}} \tag{40}$$

Using (39) and (40) and the results obtained from using the LM, two set estimates of R_m and C_m were found, one for when the vesicle is active via switching, the other for when the cell is at rest. At rest or when no switching excitation is occurring,

$$\widehat{R_m} = 10.029 \ M\Omega$$

and

$$\widehat{C_m} = 5.080 \ pF$$

Using the switching excitation, going from the "on" state to the "off" state the membrane resistance capacitance are as follows:

$$\widehat{R_{mON}} = 10.032 \ M\Omega$$

$$\widehat{R_{mOFF}} = 10.106 \ M\Omega$$

where $\widehat{R_m}$ remains relatively constant while

$$\widehat{C_{mON}} = 5.580 \ pF$$

$$\widehat{C_{mOFF}} = 5.0489 \ pF$$

For the second algorithm, using the MF/CC methods, the estimates were found to be

$$\widehat{V_m} = 5.2038$$

$$\hat{\phi} = -0.3016$$

using the same procedure, the estimates for R_m and C_m were found to be

$$\widehat{R_{mON}} = 10.013 \ M\Omega$$

$$\widehat{R_{mOFF}} = 10.091 \ M\Omega$$

and

$$\widehat{C_{mON}} = 5.5041 \ pF$$

$$\widehat{C_{mOFF}} = 5.049\ pF$$

Considering the accuracy of the estimated values compared to the true values using the LSE, for the LM algorithm, R_m and C_m were found to be within 98.95% and 99.03% of the true values respectively. For the MF/CC algorithm, R_m and C_m were found to be within 99.10% and 99.03% of the true values.

Although we obtained sufficient estimates for the unknown vector, careful considerations of the problem made this practical. The selection of the input frequency was chosen by utilizing the desire to have a system that is sensitive to the conductance/susceptance ratio as a function to the excitation frequency. In doing so, f was chosen to be 1 KHz. The choice of excitation frequency can ultimately result in a tradeoff in the experiment, as seen in [7], estimates for R_m improve at lower frequencies, as seen at $f = 100\ Hz$.

3.2 Nonlinear Least-Squares

In this section the possibility of estimating the entire 3-element model is explored. Since (5) is a nonlinear function, this leads us to using a nonlinear least-squares (NLSE) estimator. Here we will explore a different approach for producing an estimator in which all of the parameter values in the 3-element model are obtained. Before proceeding any farther, the author would first like to thank Dr. Kay for his help in the derivations for this estimator.

Using the 3-element model, shown in Fig. 1, the impedance function

$$Z(s) = \frac{R_m + R_a + sR_aR_mC_m}{1 + sR_mC_m} \tag{41}$$

can be shown to be

$$Z(s) = \frac{R_a(s + \frac{R_m+R_a}{R_aR_mC_m})}{s + \frac{1}{R_mC_m}} \tag{42}$$

by factoring (41). Equation (42) can be also thought of as a transfer function, therefore by using a transformation of parameters and letting $s = j\omega$, the impedance/-

transfer function can be expressed in terms of its angular frequency ω,

$$Z(j\omega) = \frac{G(j\omega + b)}{j\omega + a} \tag{43}$$

where

$$G = R_a$$

$$b = \frac{R_m + R_a}{R_a R_m C_m}$$

$$a = \frac{1}{R_m C_m}$$

and G, b, and a are > 0. Note that (43) is a complex function, which leads us to use classical estimation methods for complex data.

For this simulation, $Z(j\omega)$ was measured at $N = 20,000$ frequencies, therefore we define our signal model as

$$\tilde{s}[n] = \tilde{Z}(j\omega_n) = \frac{G(j\omega_n + b)}{j\omega_n + a} \tag{44}$$

Since we have a complex signal model, we assume the additive Gaussian noise to also be complex, defined as

$$\tilde{w} \sim CN(0, \sigma^2)$$

or

$$\tilde{w}[n] = u[n] + jv[n]$$

where both the variables u and v are real Gaussian zero-mean random variables (RVs) with $\sigma^2 = 1$, independent of one another and each distributed as

$$u \sim N(0, \frac{\sigma^2}{2})$$

$$v \sim N(0, \frac{\sigma^2}{2})$$

Define the complex data set then as

$$\tilde{x}[n] = \tilde{s}[n] + \tilde{w}[n] \tag{45}$$

We wish to establish a maximum likelihood estimator (MLE) where the parameter values of the 3-element model can be determined by minimizing

$$\sum_{n=0}^{N-1} |\tilde{x}[n] - \tilde{s}[n]|^2 \tag{46}$$

over the ranges that G, b, and a can assume. Once the transformed parameters have been found, an inverse transformation exists such that the desired values can be obtained. Rewriting (44) as

$$\tilde{s}[n] = \frac{G(j\omega_n + b)}{j\omega_n + a} = \frac{G(j\omega_n)}{j\omega_n + a} + \frac{Gb(1)}{j\omega_n + a} \tag{47}$$

we see that the signal model is linear in the G and b parameters, but nonlinear in a. This can be recognized to be a separable least-squares problem in which is of the form the linear model assumes except the observation matrix $\mathbf{H}$ is dependent on $a = \alpha$, i.e.

$$\mathbf{s} = \mathbf{H}(\alpha)\beta \tag{48}$$

where the $N \times q$ (q = 2) matrix $\mathbf{H}$ is of the form

$$H(\alpha) = [\mathbf{h}_{1n}\mathbf{h}_{2n}]$$

$$= \begin{bmatrix} \frac{j\omega_n}{j\omega_n+a} & \frac{1}{j\omega_n+a} \end{bmatrix}$$

$$= \begin{bmatrix} \frac{j\omega[0]}{j\omega[0]+a} & \frac{1}{j\omega[0]+a} \\ \frac{j\omega[1]}{j\omega[1]+a} & \frac{1}{j\omega[1]+a} \\ \vdots & \vdots \\ \frac{j\omega[N-1]}{j\omega[N-1]+a} & \frac{1}{j\omega[N-1]+a} \end{bmatrix}$$

and $\beta = [G \quad Gb]^T$. The unknown θ is given as $\theta = [\alpha \quad \beta]^T$ where β is a $q \times 1$ vector and α is a scalar for which can be found using a course grid search [2].

The complex LSE is found by minimizing

$$J_C(\theta) = (\tilde{x} - \tilde{s})^H(\tilde{x} - \tilde{s})$$

where H denotes the complex conjugate transpose. Thus (48) can be minimized with respect to β, reducing the minimization problem down to a function of α only

$$J_C(\alpha, \beta) = (\tilde{x} - \tilde{H}(\alpha)\beta)^H(\tilde{x} - \tilde{H}(\alpha)\beta) \tag{49}$$

for which the value of β that minimizes (49) for a given α is

$$\hat{\beta} = (\tilde{H}^H(\alpha)\tilde{H}(\alpha))^{-1}\tilde{H}^H(\alpha)\tilde{x} \tag{50}$$

Plugging in (50) into the objective function (49), we have

$$J_C(\alpha, \hat{\beta}) = \tilde{x}^H\tilde{H}(\alpha)(\tilde{H}^H(\alpha)\tilde{H}(\alpha))^{-1}\tilde{H}^H(\alpha)\tilde{x} \tag{51}$$

In order to employ the use of a grid search, we must find the value of a that maximizes (51) over the range that a can take on. Since this is a transformed parameters, it is crucial that the chosen range of values is sufficient, otherwise the performance of the estimator is poor, as seen in [7]. By choice, the range chosen is from 1 to 40,000, where the true value of $a = 200$. Recall that $a = \frac{1}{R_m C_m}$ which is of course a real function, therefore when performing the grid search, use the *Real* part of (51) to determine $\hat{\alpha}$, i.e,

$$\Re(\tilde{x}^H\tilde{H}(\alpha)(\tilde{H}^H(\alpha)\tilde{H}(\alpha))^{-1}\tilde{H}^H(\alpha)\tilde{x})$$

The results of the grid search can be seen in Fig. 9, where the search yielded an estimated value of the nonlinear parameter. Once the grid search has been done, the linear LSE is found by minimizing

$$\hat{\beta} = \Re(\tilde{H}^H(\hat{\alpha})\tilde{H}(\hat{\alpha}))^{-1}\tilde{H}^H(\hat{\alpha})\tilde{x}) \tag{52}$$

where now the unknown linear parameters G and b can be determined. Recall the way we expressed the signal model in (47), which can be written of the form

$$\tilde{s}[n] = \theta_1\tilde{h}_1[n] + \theta_2\tilde{h}_2[n] \tag{53}$$

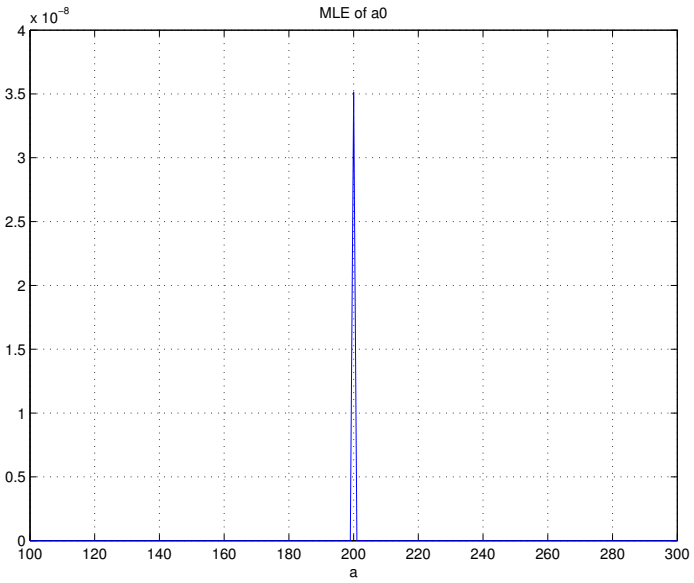

Figure 9. The result of a grid search used to determine the nonlinear parameter.

Then it follows that

$$\theta_1 = G$$

and

$$\theta_2 = Gb \Leftrightarrow b = \frac{\theta_2}{\theta_1}$$

Now that the values of the transformed parameters have been found, the parameter values of the 3-element model can be determined using an inverse transformation which is of the form

$$\widehat{R_a} = \hat{G}$$

$$\widehat{R_m} = \frac{\hat{G}}{\hat{a}}(\hat{b} - \hat{a})$$

$$\widehat{C_m} = \frac{1}{\hat{a}\widehat{R_m}}$$

3.2.1 Results for NLS

This method is extremely computationally extensive due to (51), therefore the values chosen for the 3-element model were $R_a = 20\ \Omega$, $R_m = 1\ K\Omega$, and

$C_m = 5\ \mu F$ such that the inverse of the observation matrix can be achieved in MATLAB. By choosing these values for the model, the transformed parameters were calculated to be $G = 20$, $b = 10,020$, and $a = 200$ for which the grid search yielded $\hat{a} = 201.005$, then from a single realization of the experiment, the estimates for the other two were found to be $\hat{G} = 20.022$ and $\hat{b} = 10,191$. Using this information, this brings us to the final result in which we use the inverse transformations to obtain the following results

$$\widehat{R_a} = 20.022\ \Omega$$

$$\widehat{R_m} = 995.1065\ \Omega$$

$$\widehat{C_m} = 4.9995\ \mu F$$

3.3 Conclusions

Recall that the true values of V_m and ϕ were 5.2009 and -0.3013 respectively. Using Monte-Carlo simulations we can now discuss the accuracy of the estimators discussed thus far. For the linear least-squares estimators, we describe the accuracy of the two different approaches leading up the linear LS estimator. From the results from the linear model, the accuracy of the magnitude and phase estimates were within 99.89% and 98.48% of the true values. However, using the results obtained using the MF/CC algorithm, the estimates were found to be within 99.94% and 99.91% of the true values, making this set of estimates the better of the two methods. Considering the computational time required to execute these two algorithms *on average*, we must first consider whether the switching excitation has been applied. Assuming the vesicle is in the "off" state, meaning the capacitance is constant, for the linear model, it takes 4.047 seconds. For the correlation algorithm it requires 4.374 seconds. Now taking into account when the switching excitation is applied in order to represent vesicle activity, for the linear model, it takes 4.175

seconds. For the second algorithm, to surprise actually requires a shorter time than that of constant capacitance, 4.224 seconds.

Taking into account the accuracy and run times of the algorithms presented in this chapter thus far, for the nonlinear LS estimation, the circuit parameters R_a, R_m, and C_m were found to be within 99.89%, 99.51%, and 99.99% of the true values. However, given the desire to monitor the capacitance in a real-time setting, the notion of nonlinear parameter estimation is immediately dismissed due the nonlinear equations followed by the extensive computational time required by the grid search and the inversion of the matrices (63.328 seconds). When considering the results from the linear LSE, since we also wish to monitor the presence of activity, we only consider the switching excitation sets. Although the LM set requires less time to compute, due to the better phase accuracy and parameter estimates presented by the MF/CC algorithm, it is believed that the MF/CC algorithm performs the best of the LS algorithms.

It was shown in early stages in the works of this thesis that from (35), a set of equations known the *normal* equations were found as the last step before the LSE was determined, these normal equations are given by

$$H^T H\alpha = H^T x \tag{54}$$

In original derivations, the goal was to estimate the complete 3-element model using linear LSE where the plant matrix consisted of a three column matrix with i_m, i'_m, and v'_m where the first, second, and third columns respectively. The problem with this is that with these normal equations, by including derivatives in the observation matrix, large perturbations are introduced by the process of differentiation, thus the problem became ill-conditioned. However, it was shown in [8] that using a QR factorization of the $\mathbf{A}$ matrix can lead to a LS solution if the columns of $\mathbf{A}$ are linearly independent.

List of References

[1] P. Chen and K. D. Gillis, "The noise of membrane capacitance measurements in the whole-cell recording configuration," *Biophysical Journal*, vol. 79, pp. 2162–2170, October 2000.

[2] S. M. Kay, *Fundamentals of Statistical Signal Processing: Estimation Theory*. Upper Saddle River, New Jersey, United States of America: Prentice Hall, 1993.

[3] D. C. Lay, *Linear Algebra and Its Applications , 4th. edn.* College Park, Maryland, United States of America: University of Maryland: College Park, 2012.

[4] F. A. Graybill, *Theory and Application of the Linear Model*. North Scituate, Massachusetts, United States of America: Duxbury Press, 1976.

[5] S. M. Kay, *Fundamentals of Statistical Signal Processing: Detection Theory*. Upper Saddle River, New Jersey, United States of America: Prentice Hall, 1998.

[6] S. M. Kay, *Intuitive Probability and Random Processes using MATLAB*. New York, New York, United States of America: Springer, 2006.

[7] D. W. Barnett and S. Misler, "An optimized approach to membrane capacitance estimation using dual-frequency excitation," *Biophysical Journal*, vol. 72, pp. 1641–1658, April 1997.

[8] G. Golub and C. V. Loan, *Matrix Computations, 3th. edn.* Baltimore, Maryland, United States of America: John Hopkins Press, 1996.

CHAPTER 4

Low-Pass Filter Detection

4.1 Introduction

In this chapter, a much simpler algorithm is introduced than that of the estimation algorithms seen previously. This phase change is detected by multiplying two voltage waveforms followed by low-pass filtering. Using several well known low-pass filters, an evaluation was conducted to determine which performed best, including Butterworth, Chebyshev, and elliptic (Cauer).

Defining the waveforms used by the signal processing algorithm, the input voltage is given by

$$v_m = V_m sin(\omega t) \tag{55}$$

with magnitude V_m and the output voltage as

$$v = V sin(\omega t + \phi) \tag{56}$$

with magnitude V, both of which are have an input frequency f of 1 KHz and where $\omega = 2\pi f$ is the angular frequency (rads/sec) and ϕ is the phase shift that we are interested in. This algorithm uses a simpler approach than that of the least-squares approach by multiplication of (55) and (56) and using the trigonometric identity

$$\sin(\alpha)\sin(\beta) = \frac{1}{2}[cos(\alpha - \beta) - cos(\alpha + \beta)]$$

where $\alpha = \omega t$ and $\beta = \omega t + \phi$. In doing so we have

$$\frac{V_m V}{2}[cos(\phi) - cos(2\omega t + \phi)] \tag{57}$$

where $cos(\phi)$ is the low-frequency component, while $cos(2\omega t + \phi)$ is the high-frequency component which we wish to remove. By designing a proper LPF, the

high-frequency component will be filtered such that any "glitch" in the output is representative of vesicle activity. This is due to the fact that the vesicle activity is related to the momentary changes in the surface area of the cell membrane during the cellular transport processes. This is due to the lipid bilayer having a constant capacitance at rest. However during vesicle activity, the membrane capacitance increases as a result of the increasing surface area, thus, a proportional relationship between the two quantities.

For this experiment, we define the signal model by the multiplication of the input and output voltages to be

$$s[n] = v_m[n]v[n] \tag{58}$$

We also define the noisy data set to be

$$x[n] = s[n] + w[n] \tag{59}$$

where $w[n]$ is WGN with zero mean and variance $\sigma^2 = 0.01$. The multiplicative output of the two signals can be seen in Fig. 10.

4.2 Continuous-Time Filters

4.2.1 Butterworth Filters

The Butterworth filter is known to have a frequency (magnitude) response that is *maximally flat* in passband as well as the stopband.

The continuous squared magnitude response is given by

$$|H_c(j\omega)|^2 = \frac{1}{1 + (\frac{\omega}{\omega_c})^{2N}} \tag{60}$$

where ω_c is the cutoff frequency and N is the filter order. Note that $|H_c(j\omega)|$ is a montonically decreasing function for all ω, thus reinforcing monotonicity in both the passband and stopband. Shown in Fig. 11 is the magnitude response for a 6th order Butterworth filter where for $\omega \gg \omega_c$, $|H_c(j\omega)|$ has a rolloff rate of -20N dB per decade (dB/dec).

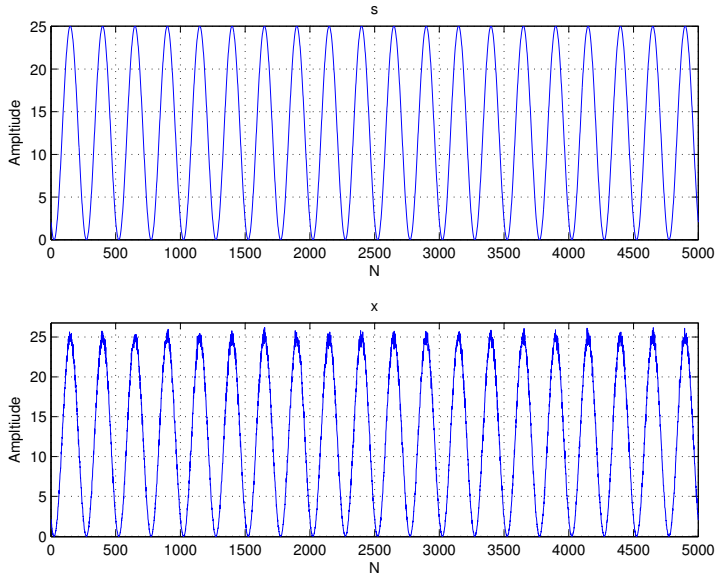

Figure 10. Signal models used in the low-pass detection algorithm.

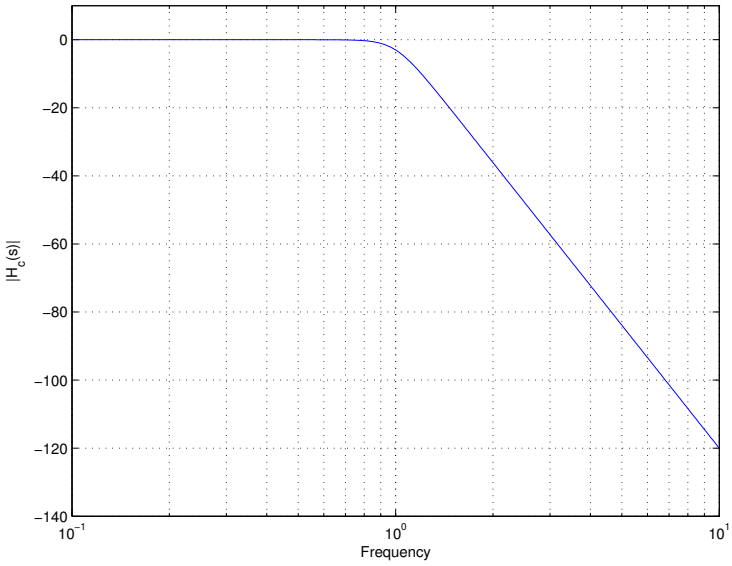

Figure 11. Magnitude response for a 6th order Butterworth filter on a logarithmic scale.

By definition

$$|H_c(j\omega)|^2 = H_c(j\omega)H_c^*(j\omega) = H_c(j\omega)H_c(-j\omega)$$

where $*$ denotes the complex conjugate, also satisfies the continuous-time equation by setting $j\omega = s$

$$H_c(s)H_c(-s) = \frac{1}{1 + (\frac{s}{j\omega_c})^{2N}} \tag{61}$$

from which by setting the auxillary equation to zero, the 2N poles of (61) can be found by

$$p_k = (-1)^{\frac{1}{2N}}(j\omega_c). \tag{62}$$

Let $-1 = \exp^{j\pi(2k-1)}$ and $j = \exp^{j\frac{\pi}{2}}$ then (62) can be written as

$$p_k = \omega_c \exp^{j(\frac{\pi}{2} + \frac{(2k-1)\pi}{2N})} \tag{63}$$

From (62), the 2N poles are equally spaced $\frac{\pi}{N}$ radians around the circumference unit circle in the s-plane. However we are only interested in filters that have stability and are of the casual type, therefore the N poles chosen for $H_c(s)$ exist in the left-half plane (LHP), shown in Fig. 12 are found to be

$$p_{1,2} = -0.2588 \pm 0.9659i$$

$$p_{3,4} = -0.7071 \pm 0.7071i$$

$$p_{5,6} = -0.9659 \pm 0.2588i$$

Note that the poles with imaginary parts occur in complex conjugate pairs. The reason being why the LHP poles are chosen is explained further when discussing the bilinear transformation. Also note that from (61), $H_c(s)$ has only zeros at infinity, therefore a Butterworth filter is known to be an all-pole continuous-time filter design.

4.2.2 Chebyshev Filters

Chebyshev filters have the capability of achieving a faster rolloff rate near ω_c at a tradeoff that monotonicity is lost in either the passband or the stopband.

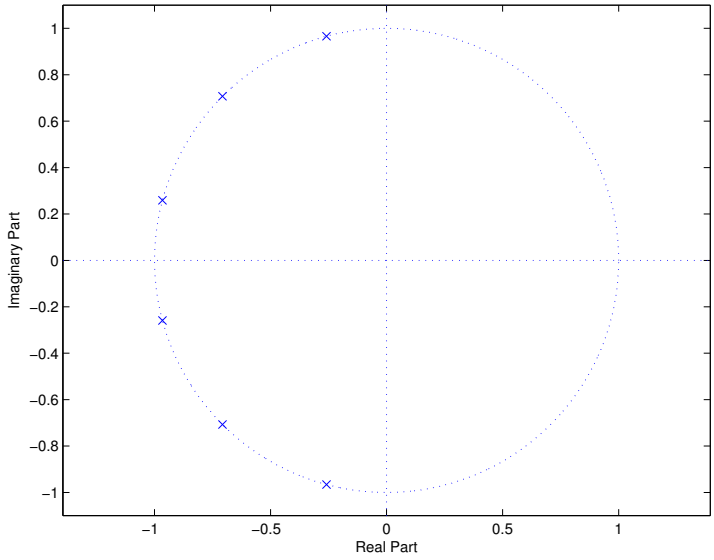

Figure 12. Pole locations of $H_c(s)$ for a 6th order Butterworth filter.

The Chebyshev filter designs are classified into two categories: Type 1 and Type 2. However, for this thesis we will only be focusing on type 1 designs. Shown in Fig. 14, a Chebyshev-I filter is known to have equiripple is the passband, while remaining monotonic in the stopband with a rolloff rate of approximately -130 dB/dec, slighty faster than the -120 dB/dec of the Butterworth design as expected.

The continuous squared magnitude response is given by

$$|H_c(j\omega)|^2 = \frac{1}{1 + \varepsilon^2 T_N^2(\frac{\omega}{\omega_c})} \tag{64}$$

where $T_N(x)$ is a Nth order Chebyshev polynomial, defined as

$$T_N(x) = cos(N \arccos x) = \cosh[N \cosh x]$$

where $T(x)$ can be generated recursively, given by

$$T_{N+1}(x) = 2xT_N(x) - T_{N-1}(x)$$

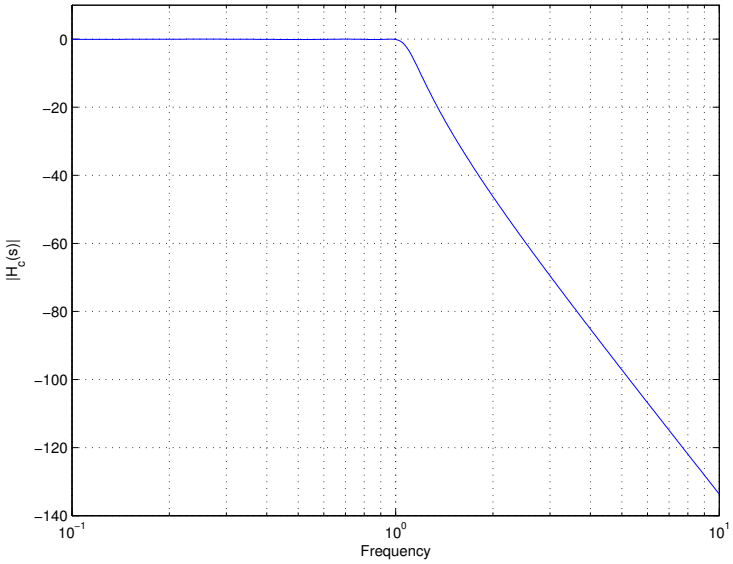

Figure 13. Magnitude Response for a 6th order Type-1 Chebyshev filter.

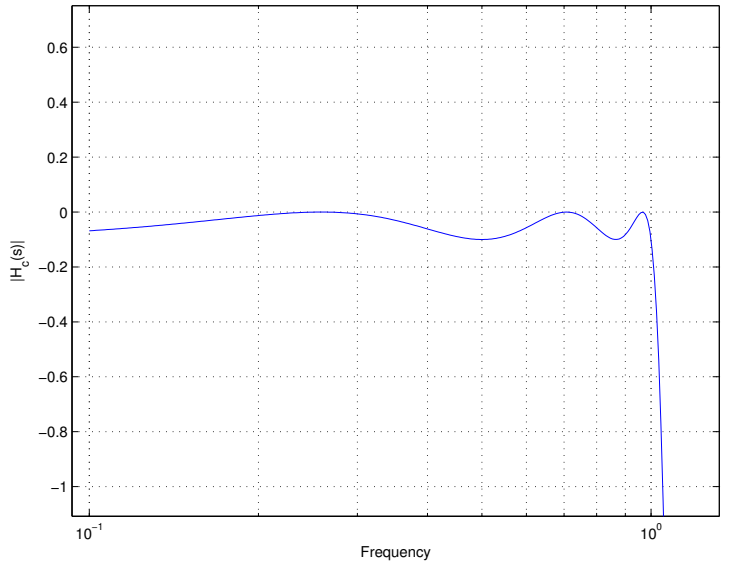

Figure 14. Equiripple in the passband of 0.1 dB in the Chebyshev and elliptic filters.

and ε^2 is determined by the passband ripple δ_1 by

$$\varepsilon^2 = \frac{1}{(1-\delta_1)^2} - 1$$

where δ_1 was chosen to be 0.1 dB.

The pole locations shown in Fig. 15, of $H_c(s)$ contain closed form solutions and from [1] are given by

$$\gamma = (\frac{1+\sqrt{1+\varepsilon^2}}{\varepsilon})^{\frac{1}{N}}$$

$$\sinh(\phi) = \frac{\gamma - \gamma^{-1}}{2}$$

$$\cosh(\phi) = \frac{\gamma + \gamma^{-1}}{2}$$

$$\mu_k = \frac{(2k-1)\pi}{2N}$$

$$\sigma_k = -(\sinh(\phi)\sin(\mu_k))\omega_c$$

$$\Omega_k = \omega_c \cosh^2(\phi) - \sigma_k^2 \coth^2(\phi)$$

then the poles are given by

$$\sigma_k + j\Omega_k$$

where

$$p_{1,2} = -0.1147 \pm 1.0565i$$

$$p_{3,4} = -0.3133 \pm 0.7734i$$

$$p_{5,6} = -0.4280 \pm 0.2831i$$

and lie in the LHP of the s-plane to guarantee stability. Again, the zeros of $H_c(s)$ lie all at infinity for a type-1 filter, therefore making this continuous-time filter an all pole design as well.

4.2.3 Elliptic Filters

Given a passband ripple and a stopband attenuation, the sharpest transition can be achieved by using a elliptic filter design. Actually, it is optimum in the sense that both the passband and stopband contain equiripple which can be seen in Fig. 16 with a passband ripple of 0.1 dB and a stopband attenuation of -60 dB.

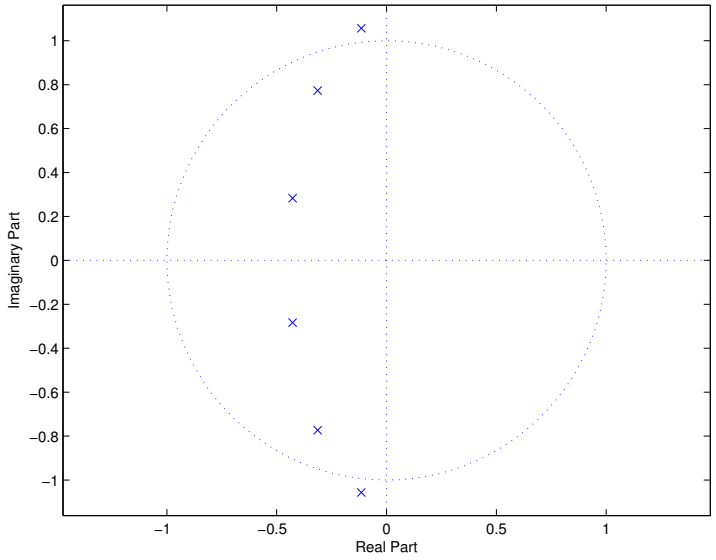

Figure 15. Pole locations of $H_c(s)$ for a 6th order Type-1 Chebyshev filter.

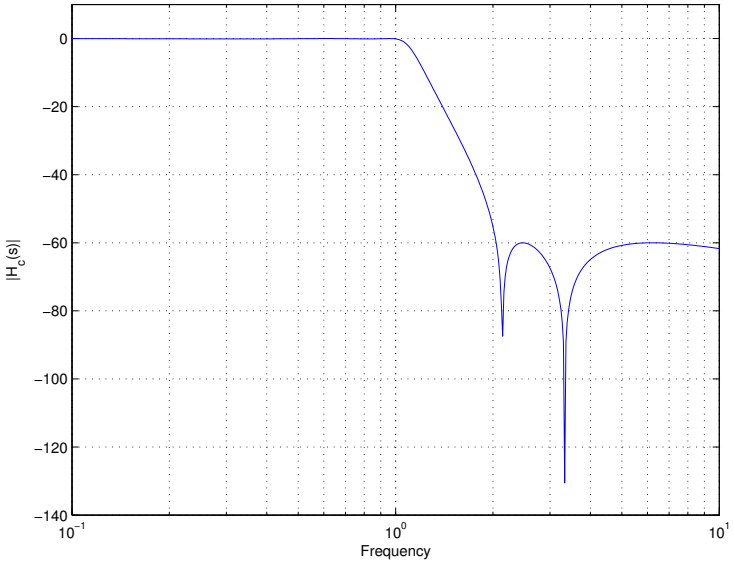

Figure 16. Magnitude response for a 5th order elliptic filter.

Similar to (64) , the squared magnitude response is given as

$$|H_c(j\omega)|^2 = \frac{1}{1+\varepsilon^2 U_N^2(\frac{\omega}{\omega_c})} \tag{65}$$

The difference being that T_N is replaced with U_N where $U_N(\omega)$ is a Jacobian elliptic

function. Therefore, our next discussion will be the pole location of $H_c(s)$. Again, the N pole locations, seen in Fig. 17, are located in the LHP of the s-plane, located at

$$p_{1,2} = -0.1402 \pm 1.0739i$$

$$p_{3,4} = -0.4295 \pm 0.7187i$$

$$p_5 = -0.5883$$

Note that the zeros of $H_c(s)$ are located on the $j\omega$ axis and occur in complex conjugate pairs at

$$z_{1,2} = \pm 2.1363i$$

$$z_{3,4} = \pm 3.3302i$$

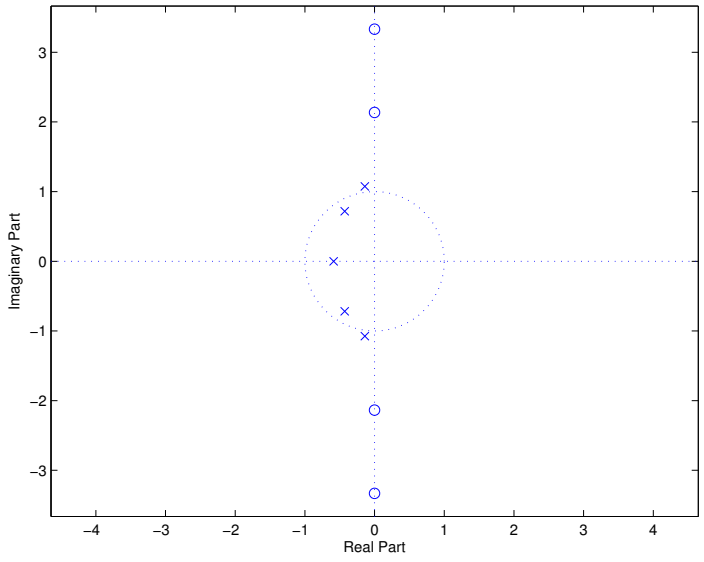

Figure 17. Pole locations for a 5th order elliptic filter.

4.3 Transformation Methods/Discrete-Time Equivalents

Here we explore how the continuous-time filters are transformed into discrete-time filters and the effects of doing so.

Now that the poles and zeros for each analog prototype have been determined, the transfer function for each filter may be expressed as

$$H(s) = K\frac{\prod_{n=1}^{N}(s - z(n))}{\prod_{n=1}^{N}(s - p(n))} \tag{66}$$

From here, one would then form a continuous-time single-input, single-output (SISO) state-space model of the form

$$\dot{x} = Ax + Bu$$

$$y = Cx + Du$$

with input u and output y and where A, B, C, and D are known as *state* matrices, obtainable from the state variable representation of the transfer function, given by

$$H(s) = C(sI - A)^{-1}B + D \tag{67}$$

where

$$A = \left[\tfrac{-1}{C_m}(\tfrac{1}{R_a} + \tfrac{1}{R_m})\right]$$

$$B = \frac{1}{R_a C_m}$$

$$C = 1$$

$$D = 0$$

4.3.1 Bilinear Transformation

In order to convert the continuous-time filters discussed thus far into their digital equivalents, we need a mathematical mapping of variables from the s-plane into the z-plane. To avoid aliasing of the frequency response, we wish to employ a

one-to-one transformation [2]. In order to do so, we must first compress the s-plane to the s'-plane using the transformation

$$s' = \frac{2}{T}\tanh^{-1}(\frac{sT}{2}) \tag{68}$$

which is bounded by

$$-\frac{\pi}{T} \leq Im(s') \leq \frac{\pi}{T}$$

where $T = \frac{1}{f_s}$. Solving for s from (68) , we have the following

$$s = \frac{2}{T}\tanh^{-1}(\frac{s'T}{2}) \tag{69}$$

Now the s'-plane can be successfully be mapped to the z-plane without the effect of aliasing. Using the transform $z = \exp^{s'T}$ and solving for s',

$$s' = \frac{1}{T}\ln z \tag{70}$$

Substituting (70) into (69)

$$s = \frac{2}{T}\tanh(\frac{\ln z}{2}) \tag{71}$$

Equation (71) can be further simplified using

$$\tanh(x) = \frac{1-\exp^{-2x}}{1+\exp^{-2x}}$$

for which we obtain the desired transformation

$$s = \frac{2}{T}(\frac{1-z^{-1}}{1+z^{-1}}) \tag{72}$$

Therefore, to convert the analog prototype into its discrete equivalent, we use what is known as the *bilinear transformation* which is given by

$$H(z) = H_c(s)|_{s=\frac{2}{T}(\frac{1-z^{-1}}{1+z^{-1}})}. \tag{73}$$

Since the s-plane was mapped into the z-plane, similarly, so do the locations of the zeros and poles. Using (66), the bilinear transfom (73) produces

$$H(z) = K(1+z^{-1})^{N-M}\frac{\prod_{m=1}^{M}(1-z_m z^{-1})}{\prod_{k=1}^{N}(1-p_k z^{-1})} \tag{74}$$

Using (74) and the s-plane pole locations, we can now determine the pole locations for the digital equivalent filters in the z-plane.

Shown in Figs. 18, 19, and 20 are the pole locations for the discrete Butterworth, Chebyshev-I, and elliptic filters.

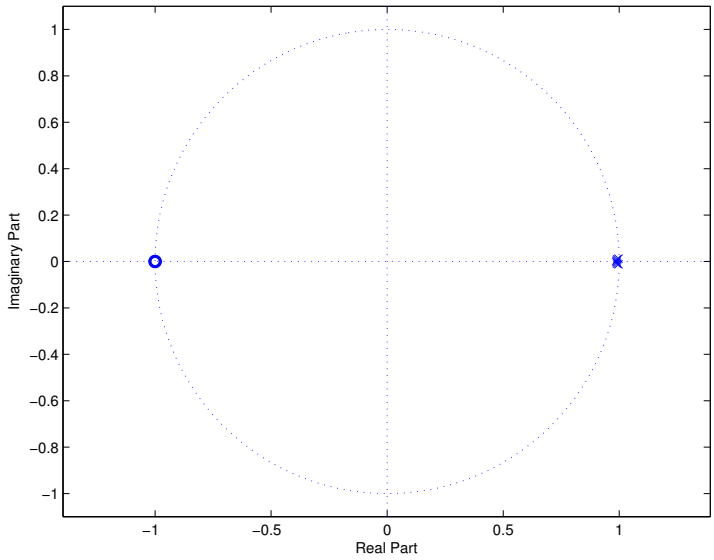

Figure 18. Pole/Zero locations for a 6th order discrete Butterworth filter.

Note that (72) is an invertible function, thus, by solving for z we have

$$z = \frac{1 + \frac{T}{2}s}{1 - \frac{T}{2}s} \tag{75}$$

From (75), for $Imag(s) = 0$, where $s = \sigma + j\omega$, $|z| = 1$ which means that for a stability criterion the $j\omega$ axis must be mapped into the unit circle by wrapping the LHP into the unit circle. In other words, by employing the bilinear transformation we have, for $\omega = 0$, $|z| = 1$ and for $\omega = \infty$, $|z| = -1$. By doing so, all the analog filter designs with zeros at infinity, the locations of the discrete equivalent zeros in $H(z)$ can be found at $|z| = -1$ and all of the poles are located inside the circle in the z-plane, guaranteeing stability.

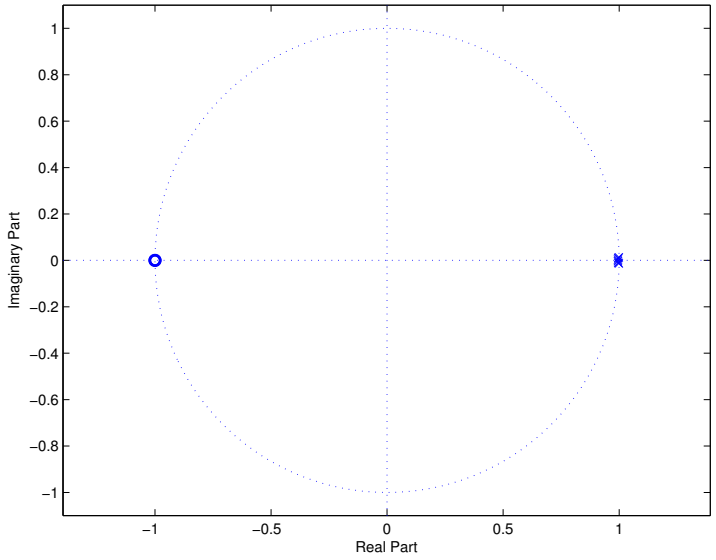

Figure 19. Pole/Zero locations for a 6th order discrete Chebyshev Type-1 filter.

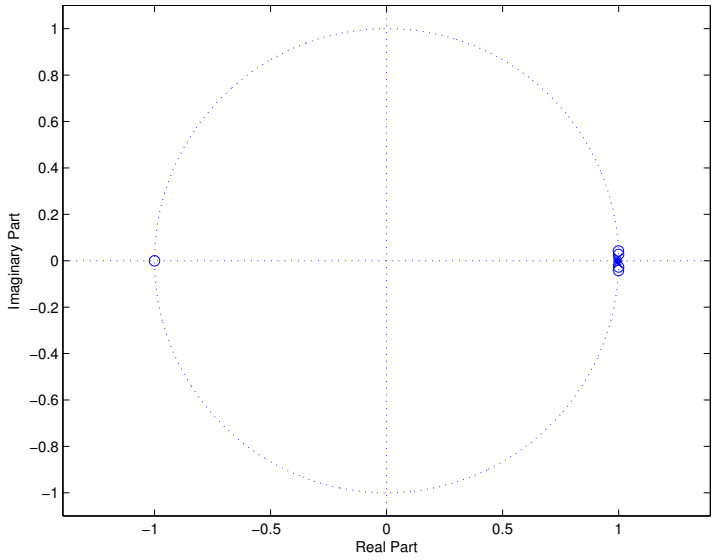

Figure 20. Pole/Zero locations for a 5th order discrete elliptic filter.

4.3.2 Frequency Warping

Recall the first step used for mapping the $j\omega$ axis in the s-plane into the unit circle of the z-plane is given by (68). Now that we know we wrap the $j\omega$ axis into

the new domain, we substitute $s = j\omega$ and $s' = j\omega'$ into (68), which gives us

$$\omega' = -\frac{2}{T}\arctan(\frac{-\omega T}{2})$$

Since the hyperbolic tangent may be expressed in terms of its inverse tangent by

$$\tanh^{-1}(x) = \frac{1}{j}\arctan(jx)$$

and since we have a negative argument of the inverse tangent, i.e.

$$\arctan(-x) = -\arctan(x)$$

we have

$$\omega' = \frac{2}{T}\arctan(\frac{\omega T}{2}) \tag{76}$$

If we now let $\Omega = \omega T$ we can see the transformation that occurs between the analog frequency and its discrete counterpart by

$$\Omega = 2\arctan(\frac{\omega T}{2}) \tag{77}$$

which is in the interval of $[0, 2\pi]$, spanning the circumference of the unit circle. The nonlinear relationship between these two quantities (ω and Ω) is known as *frequency prewarping*. The mapping of the frequencies can be determined from (73) by letting $H_c(s) = Hc(j\omega)$ where

$$\omega = \frac{2}{T}\tan(\frac{\Omega}{2}) \tag{78}$$

(found by letting $\Omega = \omega' T$ in (76)). By considering this additional transformation in filter design we can guarantee that the magnitude of the frequency response at the cut-off frequency will remain the same when the analog filter is transformed into its discrete counterpart, shown in Figs. 21, 22, and 23.

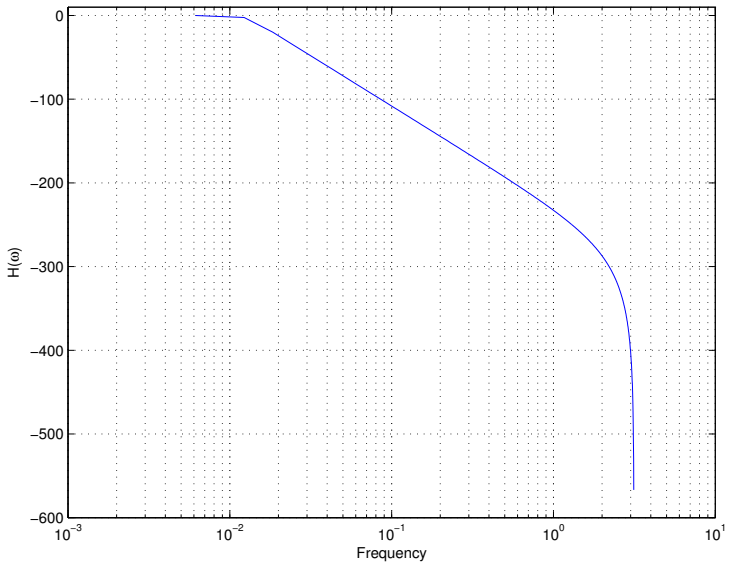

Figure 21. Magnitude Response of a 6th order discrete Butterworth filter.

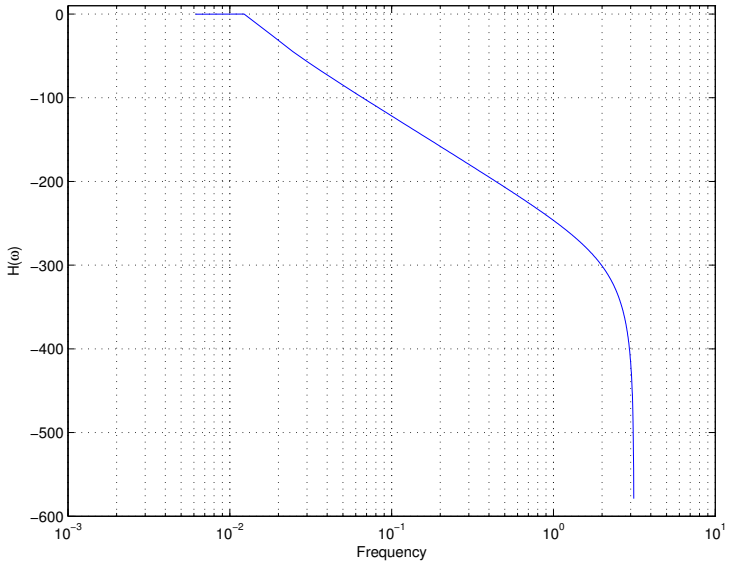

Figure 22. Magnitude Response of a 6th order discrete Chebyshev-I filter.

4.4 Conclusion

Now that the discrete equivalents of the analog prototypes have been found using the bilinear transformation, using the signals defined by (55) and (56) we

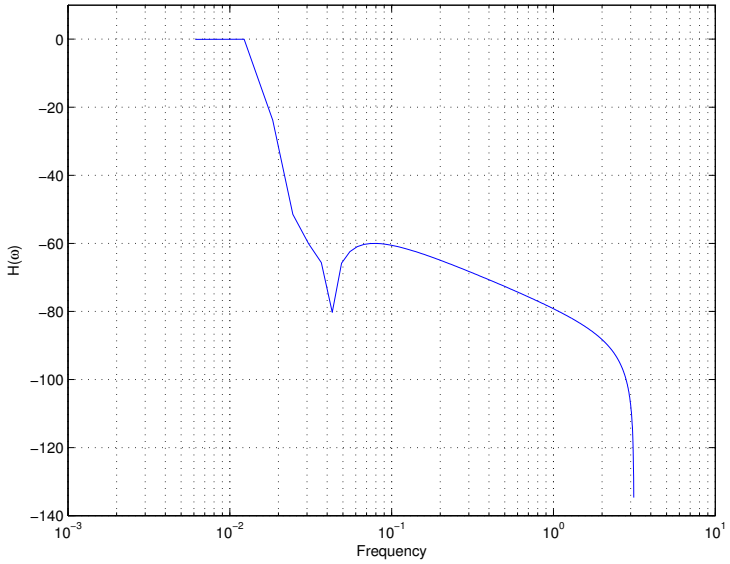

Figure 23. Magnitude Response of a 5th order discrete elliptic filter.

can now determine the how small of a change in the cell capacitance we are able to detect. Typically fusion with the vesicle is on the order of 200 ms, the recorded time of vesicle activity is decreased to 100 ms. The detectability of this algorithm relies on the human eye, therefore the change in the cell capacitance was chosen to be 100fF, values chosen less than this had biased results due to a prior knowledge of location of the "glitch".

Since good time resolution is desired in such an application, the choice of the sampling rate (frequency) was chosen to $f_s = 500KHz$, half of which what used for the linear LS estimation problem. During the filter design the argument of a normalized frequency is found to be

$$f_{normalized} = \frac{f_{in}}{f_{Nyquist}} = 0.004$$

where

$$f_{Nyquist} = \frac{f_s}{2}$$

By applying the three filter designs discussed thus far to (59), three sets of

outputs were obtained of which can be seen in Figs. 24, 25, and 26, where it was

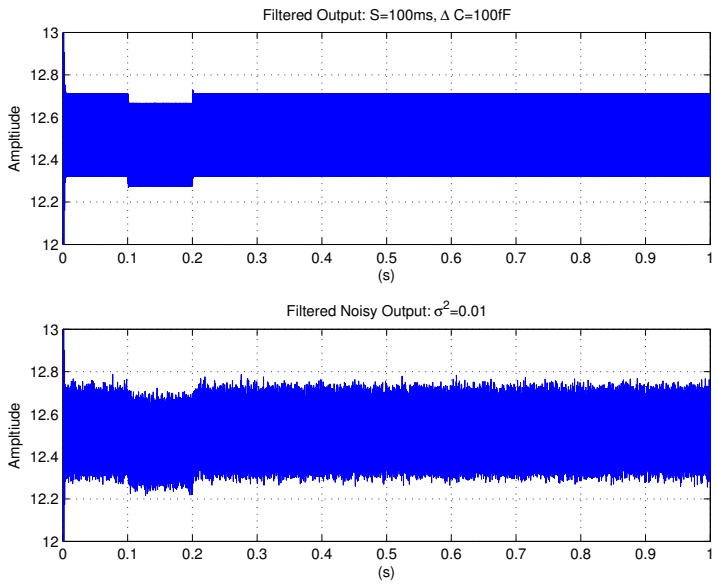

Figure 24. Filtered output using a 6th order discrete Butterworth filter.

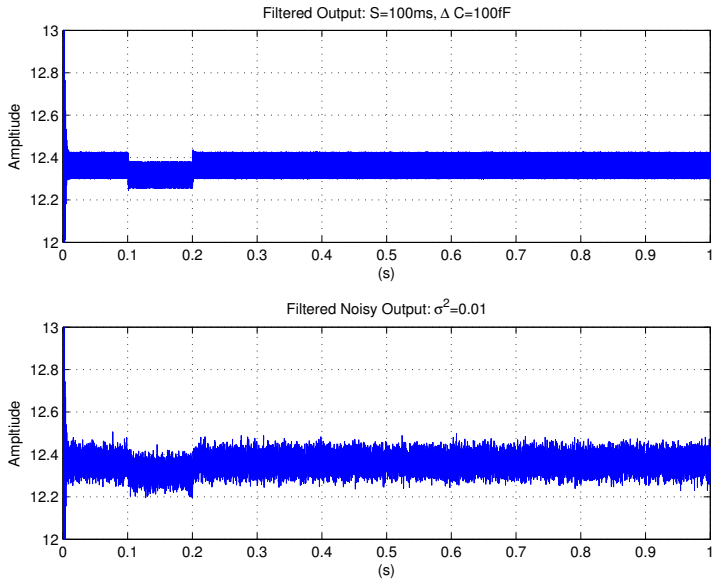

Figure 25. Filtered output using a 6th order discrete Chebyshev-I filter.

determined that the Butterworth filter performed the poorest while the elliptic filter performed the best as expected in terms of visual detectability and could be

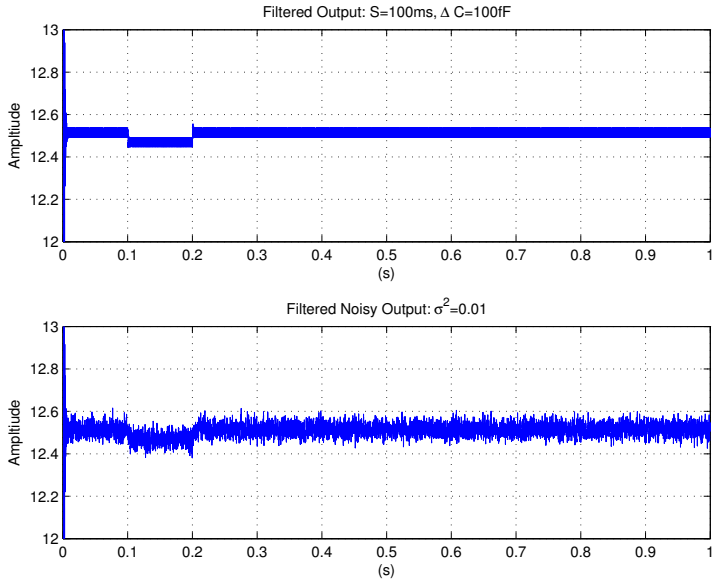

Figure 26. Filtered output using a 5th order discrete elliptic filter.

achieved using a lower order filter than that of the other two designs as expected. In terms of run times, the Butterworth took the least amount of time to execute, at 2.784 seconds. For the Chebyshev, due to the polynomial, the time required was 2.822 seconds. Lastly, due to the complexity of the Jacobian function associated with the elliptic filter, the run time was 2.996 seconds. Based on this, it is clear that the detection algorithms are faster than that of the estimation ones seen in the previous chapter.

One last measure of comparison used in determining the performance of these three filters, the signal-to-noise ratio (SNR) of the filtered output was obtained, the SNR defined to be the ratio summed squared-magnitude or power of the signal to that of the power of the noise, i.e.,

$$SNR = \frac{P_{Signal}}{P_{Noise}}$$

The Butterworth was found to have the largest, at 41.9512 decibals (dB), while the Chebyshev-I and elliptic filters were found to be 41.8372 and 41.9474 dB.

List of References

[1] L. B. Jackson, *Digital Filters and Signal Processing with MATLAB Exercises*. Norwell, Massachusetts, United States of America: Kluwer Academic Publishers, 1996.

[2] L. B. Jackson, *Signals, Systems, and Transforms*. Norwell, Massachusetts, United States of America: Kluwer Academic Publishers, 1991.

APPENDIX A

Derivation of Estimator

The linear model follows that the data x can be written in the vector form

$$x = H\alpha + w$$

Since the assumption has been made that the noise PDF is Gaussian, the PDF which can be expressed in matrix/vector notation

$$p(x;\alpha) = \frac{1}{(2\pi\sigma^2)^{N/2}} \exp^{-\frac{1}{2\sigma^2}(x-H\alpha)^T(x-H\alpha)}$$

Taking the natural logarithm of $p(x;\alpha)$

$$\ln p(x;\alpha) = -\ln((2\pi\sigma^2)^{N/2}) - \frac{1}{2\sigma^2}(x-H\alpha)^T(x-H\alpha)$$

and then taking the partial derivative with respect to α is given by

$$\frac{\delta \ln p(x;\alpha)}{\delta\alpha} = -\frac{1}{2\sigma^2}\frac{\delta}{\delta\alpha}(x^Tx - 2x^TH\alpha + \alpha^TH^TH\alpha).$$

Now let $x^TH = b^T$ and let $H^TH = A$, then using the identities

$$\frac{\delta b^T\alpha}{\delta\alpha} = b$$

and

$$\frac{\delta\alpha^TA\alpha}{\delta\alpha} = 2A\alpha$$

we have the following

$$\frac{1}{\sigma^2}(H^Tx - H^TH\alpha)$$

for which by setting equal to zero and solving for α produces our LSE, which is given by

$$\widehat{\alpha} = (H^TH)^{-1}H^Tx$$

APPENDIX B

MATLAB Code

```
clear all; clc; close all;
randn('state',0);

f=1000; % input freq @ 1 KHz
fs=1e6;

w=2*pi*f; % angular freq (rads/sec)
t=[0:1/fs:(1-1/fs)]'; % 1s, fs = 1MHz
N=length(t); % # of samples = 1,000,000

Im=500e-9; % injection current
im=Im*sin(w*t); % input

% parameters
Ra=1e6; % access resistance
Rm=10e6; % membrane resistance
C=5e-12; % static membrane capacitance
Rt=Ra+Rm;
Rp=(Ra*Rm)/Rt;

Cm=zeros(N,1);
S=[ones(0.2*N,1); zeros(0.8*N,1)]; % 20% duty cycle
deltaCm= 0.5e-12;

for i = 1:0.2*N % 0.0 -> 0.2 (seconds)
    Cm(i,1)=C+(0*deltaCm); % vesicle is on
```

```
end
for j =(0.2*N+1):N % 0.2 -> 1.0 (seconds)
    Cm(j,1)=C; % keep fixed (vesicle is off)
end

Real=(1+(w^2)*Rm*Rp*(Cm.^2))./(Rt*(1+(w^2)*(Rp^2)*(Cm.^2)));%conductance
Imag=(w*(Rm^2)*Cm)./(Rt^2*(1+(w^2)*(Rp^2)*(Cm.^2)));%susceptance
Admit=Real + j*Imag; % admittance function
Admit_mag=1./sqrt(Real.^2 + Imag.^2); % siemens (ohm^-1)
Admit_phase=atan(Imag./Real); % radians

% using phasors
Vm=Im.*Admit_mag; % vm magnitude
phi= 0 - Admit_phase; % vm phase
vm=Vm.*sin(w*t + phi); % induced waveform
v=vm-im*Ra; % ohm's law

T= 5000; % 5 cycles
var= 1; wgn=sqrt(var)*randn(N,1); % noise~N(0,var)
data=vm+wgn; % add WGN to vm (from A/D)

% alt. (Kay v1)
H1=[sin(w*t(1:T)), cos(w*t(1:T))]; % on
alpha_hat1=inv(transpose(H1)*H1)*transpose(H1)*data(1:T);
A_est1=sqrt(alpha_hat1(1,1)^2 + alpha_hat1(2,1)^2);
P_est1=-atan(-alpha_hat1(2,1)/alpha_hat1(1,1));
%
H2=[sin(w*t(40*T+1:41*T)), cos(w*t(40*T+1:41*T))]; % off
alpha_hat2=inv(transpose(H2)*H2)*transpose(H2)*data(40*T+1:41*T);
A_est2=sqrt(alpha_hat2(1,1)^2 + alpha_hat2(2,1)^2);
P_est2=-atan(-alpha_hat2(2,1)/alpha_hat2(1,1));
```

```
% extract magnitude/phase information ( on )
vm_ud=flipud(vm(1:T)); % flipped/shifted signal
mfilt=conv(data(1:T),vm_ud); % convolve noisy signal with "match"
mfilt=[mfilt; 0]; % zero pad
mag_real=max(vm(1:T)); % amplitude of induced voltage
mag_est=sqrt((2*max(mfilt))/length(t(1:T))); % estimate of amp from MF

[cc,lag_samples]=xcorr(im(1:T),data(1:T)); % compute cross-correlation
cc=[cc; 0]; lag_samples=[lag_samples'; 0]; % zero pad
[~,lag_max]=max( cc( ((length(cc))/2):end) ); % find delay
% visual search for max, if lag_sample used, error...
true=-48;
phase_est= 2*pi*(true)/f; % radians/sec


vm_est=A_est1*sin(w*t + phase_est); % signal estimate used in LSE

% LSE
im_prime=w.*Im.*cos(w*t); % d/dt(im)
vm_prime=w.*mag_est.*cos(w*t +phase_est); % d/dt(vm)
x = vm_prime(1:T) - Ra*im_prime(1:T); % derivative variable

% % cycles 1-5 ( on )
A1=[im(1:T), vm_est(1:T)]; % plant matrix
theta1=(transpose(A1)*A1)\(transpose(A1)*x); % estimator
Rm_est1= -(theta1(1,1)/theta1(2,1)) - Ra
Cm_est1= 1/(theta1(1,1)+(Ra*theta1(2,1)))
% % cycles 6-10
% A2=[im(T+1:2*T), vm_est(T+1:2*T)]; % plant matrix
% theta2=(transpose(A2)*A2)\(transpose(A2)*x); % estimator
% Rm_est2= -(theta2(1,1)/theta2(2,1)) - Ra ;
```

```
% Cm_est2= 1/(theta2(1,1)+(Ra*theta2(2,1)));
% 5 cycles when vesicle is off
A3=[im(40*T+1:41*T), vm(40*T+1:41*T)]; % plant matrix
theta3=(transpose(A3)*A3)\(transpose(A3)*x); % estimator
Rm_est3= -(theta3(1,1)/theta3(2,1)) - Ra
Cm_est3= 1/(theta3(1,1)+(Ra*theta3(2,1)))
%
% % estimate vector per vesicle activity
% Rm_est_wgn=[Rm_est1;Rm_est2;Rm_est3]
% Cm_est_wgn=[Cm_est1;Cm_est2;Cm_est3]

% % FFT
% F=(2/N)*abs(fft(v));
% F=F(1:(end/2));
% figure; plot(F);

% % mag accuracy
% acc1=mag_real/A_est1; % accuracy of LM to true
% acc2=mag_real/mag_est; % accuracy of MF to true
%
% % phase accuracy
% acc3=phi(1)/P_est1; % accuracy of LM to true
% acc4=phi(1)/phase_est; % accuracy of CC to true

% figure;
% subplot(311);
% plot(t,S); grid on;
% xlabel('t'); ylabel('Amplitude');
% axis([0 1 0 1.5]);
% title('RC0');
% % subplot(312); plot(t,-S); grid on;
% % xlabel('t'); ylabel('Amplitude');
```

```
% % title('RC1');
% subplot(313); plot(t,Cm); grid on;
% xlabel('t'); ylabel('Amplitude');
% title('Membrane Capacitance due to Switching');

% figure; plot(t,im); grid on;
% axis([0 0.001 -6e-7 6e-7]);
%
% figure; plot(t,data); grid on;
% axis([0 0.001 -8 8]);

% figure; plot(t,Rm*im,t,vm,'r',t,v,'g'); grid on;
% axis([0 0.005 -6 6]); legend('i_m','v_m','v');

% figure;
% subplot(211); plot(t,vm); grid on;
% axis([0.19 0.21 -6 6]);
% subplot(212); plot(t, v); grid on;
% axis([0.19 0.21 -6 6]);

% figure;
% plot(v(1:5000)); hold on; % on
% plot(v(20000:25000),'r'); grid on; % off
% xlabel('1 cycle = 1000 samples');
% ylabel('V'); title('v');
% legend('Cycles 1-5, vesicle on','Cycles 20-25, vesicle off',4);

% figure;
% plot(1:length(mfilt),mfilt); grid on;
% xlabel('N'); ylabel('Amplitude');
% %title('Matched Filter Output');
% figure;
```

```
% plot(lag_samples,cc); grid on; % plot lag vs correlation
% xlabel('Lag Sample'); ylabel('Correlation Value');
% %title('Cross Correlator Output');

% figure;
% plot(t,vm,t,vm_est,'r'); grid on;
% xlabel('t'); ylabel('Amplitude');
% %title('v_m vs. v_m estimate');
% axis([0 0.001 -6 6]); legend('vm','vm est');



% Stephen Sladen
% LPF algorithm

clear all; clc; close all;
randn('state',0);
f_input=1e3;
%f_sampling=1e6;
f_sampling=500e3;
f_nyquist=f_sampling/2;
f_normalized=f_input/f_nyquist;
w=2*pi*f_input; % angular freq (rads/sec)
t=[0:1/f_sampling:(1-1/f_sampling)]'; % 1s, fs = 1MHz
N=length(t); % # of samples = 500,000
T=5e3; % 10 cycles
Im=500e-9; % injection current
im=Im*sin(w*t); % input
Ra=1e6; % access resistance
Rm=10e6; % membrane resistance
C=5e-12; % static membrane capacitance
Rt=Ra+Rm;
Rp=(Ra*Rm)/Rt;
```

```
%this is where DELTA_C, pulse widths, and variances are changed
sig=0.01; wgn=sqrt(sig)*randn(N,1);
delta = 100e-15; % 100fF
% S1=[ones(0.2*N,1); zeros(0.8*N,1)]; % 20% duty cycle
% S3=[ones(0.5*N,1); zeros(0.5*N,1)]; % 50% duty cycle
% S1=[ones(0.001*N,1); zeros(0.999*N,1)]; % 1ms
% S2=[ones(0.005*N,1); zeros(0.995*N,1)]; % 5ms
% S3=[ones(0.010*N,1); zeros(0.990*N,1)]; % 10ms
% figure; plot(t,S1,t,S2,t,S3);
% P1=0.010*N; % 10ms
% P2=0.020*N; % 20ms
% P3=0.050*N; % 50ms (into signal)
% when setting up Cm it is dependent on the delta and the pulse widths
Cm=zeros(N,1);
% for i = 1:(P3)
%     Cm(i,1)=C+delta3; % vesicle is on
% end
% for j =(P3+1):N
%     Cm(j,1)=C; % keep fixed (vesicle is off)
% end
for i = 1:0.1*N
    Cm(i,1)=C; % vesicle is off
end
for j =(0.1*N+1):0.2*N % (100ms)
    Cm(j,1)=C+delta; % vesicle is on
end
for ii =(0.2*N+1):1.00*N
    Cm(ii,1)=C; % vesicle is off
end
Real=(1+(w^2)*Rm*Rp*(Cm.^2))./(Rt*(1+(w^2)*(Rp^2)*(Cm.^2)));%conductance
Imag=(w*(Rm^2)*Cm)./(Rt^2*(1+(w^2)*(Rp^2)*(Cm.^2)));%susceptance
% Admit=Real + j*Imag; % admittance function
```

```
Admit_mag=1./sqrt(Real.^2 + Imag.^2); % siemens (ohm^-1)
Admit_phase=atan(Imag./Real); % radians
Vm = Im.*Admit_mag; % vm magnitude
phi = 0 - Admit_phase; % vm phase
vm = Vm.*sin(w*t + phi); % induced waveform
v = vm-im*Ra; % ohm's law
x=vm+wgn; % data
% multiplication of sinusoids
B1=vm.*v; % clean
B2=x.*v; % noisy
% FILTERS (choose one at a time)
% Rp decibels of peak-to-peak ripple and a
% minimum stopband atenuation of Rs decibels.
%[b,a] = ellip(5,0.1,60,f_normalized); % ELLIPTIC
% R decibels of peak-to-peak ripple in the passband
[b,a] = cheby1(6,0.1,f_normalized); % CHEBYSHEV
%[b,a]=butter(6,f_normalized); %BUTTERWORTH
% filter output
y1=filter(b,a,B1); % clean
y2=filter(b,a,B2); % noisy

%swratio=snr(y1,wgn);

% figure; plot(Rm*im); grid on; hold on;
% plot(vm,'r'); plot(v,'g'); hold off;
% xlabel('N'); axis([0 T -6 6]); legend('im (scaled)','vm','v');
% figure; % SIGNALS
% subplot(211); plot(B1); grid on;
% xlabel('N'); ylabel('Ampltiude'); title('s');
% axis([0 T min(B1) max(B1)]);
% subplot(212); plot(B2); grid on;
% xlabel('N'); ylabel('Ampltiude'); title('x');
```

```
% axis([0 T min(B2) max(B2)]);
figure; % FILTER RESULTS!
subplot(211); plot(t,y1); grid on;
xlabel('(s)'); ylabel('Ampltiude');
title('Filtered Output: S=100ms, \Delta C=100fF');
axis([0 1 12 13]);
subplot(212); plot(t,y2); grid on;
xlabel('(s)'); ylabel('Ampltiude');
title('Filtered Noisy Output: \sigma^2=0.01');
axis([0 1 12 13]);



% Stephen Sladen
% NLS Algorithm

clear all; clc; close all;
Ra=20; % access resistance
Rm=1000; % membrane resistance %*!
Cm=5e-6; % membrane capacitance %*!
Rt=Ra+Rm;
Rp=(Ra*Rm)/Rt;
tau=Rm*Cm; % time constant
f=linspace(100,10000,20000); f=f';
wn=2*pi*f; % vector of angluar frequencies
N=length(f); % # of samples
% transformed parameters
G=Ra; % gain
b=Rt/(Ra*tau); % zero
a0=1/tau; % pole
%randn('state',0);
var=1;
w=sqrt(var)*randn(N,1); % WGN
```

```
u=sqrt(var/2)*randn(N,1);
v=sqrt(var/2)*randn(N,1);
cw=u+j*v; % CWGN
s=G*((j*wn) + b)./((j*wn) + a0); % impedance
x=s+cw;
%beta=[G ; G*b];
%alpha=a0; % bounded by time constant
a=[1:(2*N)]'; % range of values a0 can take (changes performance)
mle_a=zeros(length(a),1);
for i = 1:length(a) % estimate tau

    h1=(j*wn)./((j*wn) + a(i,1));
    h2=1./((j*wn) + a(i,1));
    H=[h1 , h2]; % dependent on alpha

    AT=[x'*h1 , x'*h2]; % transpose
    A=[x'*h1 , x'*h2]';
    Q=[h1'*h1 , h1'*h2 ; h2'*h1 , h2'*h2]^-1;

    mle_a(i,1)= real(AT*Q*A); % exact

end
a_hat=1/(find(mle_a==max(mle_a))/(length(a)));
figure; plot(a,(1/mle_a)); grid on;
xlabel('a'); title('MLE of a0');
axis([100 300 0 4e-8]);
h1_a=(j*wn)./((j*wn) + a_hat);
h2_a=1./((j*wn) + a_hat);
H_a=[h1_a , h2_a]; % dependent on alpha(hat)
theta=real(inv(H_a'*H_a)*H_a'*x);
G_hat=theta(1,1);
b_hat=theta(2,1)/theta(1,1);
```

```
Ra_hat=(G_hat)

Rm_hat=((G_hat/a_hat)*(b_hat-a_hat))

Cm_hat=(1/(a_hat*Rm_hat))
```

BIBLIOGRAPHY

"Best method to extract phase shift between 2 sinosoids, from data provided." 2015. [Online]. Available: http://dsp.stackexchange.com/questions/8673/best-method-to-extract-phase-shift-between-2-sinosoids-from-data-provided

Attia, J. O., *Electronics and Circuit Analysis using MATLAB*. Boca Raton, Florida, United States of America: CRC Press, 1999.

Barnett, D. W. and Misler, S., "An optimized approach to membrane capacitance estimation using dual-frequency excitation," *Biophysical Journal*, vol. 72, pp. 1641–1658, April 1997.

Chen, P. and Gillis, K. D., "The noise of membrane capacitance measurements in the whole-cell recording configuration," *Biophysical Journal*, vol. 79, pp. 2162–2170, October 2000.

Cullen, J., Patel, P., Shannon, J., Chabot, E., and Sun, Y., "Instrumentation for cell capacitance measurements," in *Proceedings of the 40th Annual Northeast Bioengineering Conference*. Boston, MA: IEEE, April 2014, pp. 1–2.

Debus, K., Hartmann, J., Kilic, G., and Lindau, M., "Influence of conductance changes on patch clamp capacitance measurements using a lock-in amplifier and limitations of the phase tracking technique," *Biophysical Journal*, vol. 69, pp. 2808–2822, December 1995.

Donnelly, D. F., "A novel method for rapid measurements of membrane resistance, capacitance, and access resistance," *Biophysical Journal*, vol. 66, pp. 873–877, March 1994.

Fidler, N. and Fernandez, J. M., "Phase tracking: an improved phase detection technique for cell membrane capacitance measurements," *Biophysical Journal*, vol. 56, pp. 1153–1162, December 1989.

Finkel, A. S. and Redman, S. J., "Theory and operation of a single microelectrode voltage clamp," *Journal of Neuroscience*, vol. 11, pp. 101–127, 1984.

Frasca, S. "Basic tool for periodic signal detection." December 1998. [Online]. Available: http://dsp-book.narod.ru/dad_per_basic.pdf

Golowasch, J. and Nadim, F., "Capacitance, membrane," in *Encyclopedia of Computational Neuroscience*. Springer New York, May 2014, pp. 1–5.

Golowasch, J., Thomas, G., Taylor, A. L., Patel, A., Pineda, A., Khalil, C., and Nadim, F., "Membrane capacitance measurements revisited: Dependence of capacitance value on measurement method in nonisopotential neurons," *Journal of Neurophysiology*, no. 102, pp. 2161–2175, July 2009.

Golub, G. and Loan, C. V., *Matrix Computations, 3th. edn.* Baltimore, Maryland, United States of America: John Hopkins Press, 1996.

Graybill, F. A., *Theory and Application of the Linear Model.* North Scituate, Massachusetts, United States of America: Duxbury Press, 1976.

Hodgkin, A. L. and Huxley, A. F., "A quantitative description of membrane current and its application to conduction and excitation in nerve," *Journal of Physiology*, no. 117, pp. 500–544, March 1952.

III, J. O. S. Stanford University. "Mathematics of the discrete fourier transform (dft) with audio applications, 2nd. edn." 2015. [Online]. Available: https://www.dsprelated.com/freebooks/mdft/

Jackson, L. B., *Signals, Systems, and Transforms.* Norwell, Massachusetts, United States of America: Kluwer Academic Publishers, 1991.

Jackson, L. B., *Digital Filters and Signal Processing with MATLAB Exercises.* Norwell, Massachusetts, United States of America: Kluwer Academic Publishers, 1996.

Joshi, C. and Fernandez, J. M., "Capacitance measurements: An analysis of the phase detector technique used to study exocytosis and endocytosis," *Biophysical Journal*, vol. 53, pp. 885–892, June 1988.

Kay, S. M., *Fundamentals of Statistical Signal Processing: Estimation Theory.* Upper Saddle River, New Jersey, United States of America: Prentice Hall, 1993.

Kay, S. M., *Fundamentals of Statistical Signal Processing: Detection Theory.* Upper Saddle River, New Jersey, United States of America: Prentice Hall, 1998.

Kay, S. M., *Intuitive Probability and Random Processes using MATLAB.* New York, New York, United States of America: Springer, 2006.

Lay, D. C., *Linear Algebra and Its Applications , 4th. edn.* College Park, Maryland, United States of America: University of Maryland: College Park, 2012.

Lindau, M. and Neher, E., "Patch-clamp techniques for time-resolved capacitance measurements in single cells," *European Journal of Physiology*, no. 411, pp. 137–146, February 1988.

Neher, E. and Marty, A., "Discrete changes of cell membrane capacitance observed under conditions of enhanced secretion in bovine adrenal chromaffin cells," in *Proceedings of the National Academy of Sciences*, vol. 79, November 1982, pp. 6712–6716.

Rosenberg, L., Hammick, M., Sladen, S., Wu, J., and Sun, Y., "Development of an electrophysiological instrument for universal clamp testing," in *Proceedings of the 42th Annual Northeast Bioengineering Conference*, Vestal, NY, April 2016.

Sakmann, B. and Neher, E., *Single-Channel Recording, 2nd. edn.* New York, New York, United States of America: Springer, 2009.

Sladen, S., "On transfer function parameters embedded in complex white gaussian noise," ELE661 Final Project, April 2016.

Sladen, S., Phongsavan, A., Wu, J., Chabot, E., and Sun, Y., "Development of an electrophysiological instrument for universal clamp testing," in *Proceedings of the 39th Annual Northeast Bioengineering Conference.* Syracuse, NY: IEEE, April 2013, pp. 275–276.

Solsona, C., Innocenti, B., and Fernandez, J. M., "Regulation of exocytotic fusion by cell inflation," *Biophysical Journal*, vol. 74, pp. 1061–1073, February 1998.

Stanfield, C. L., *Principles of Human Physiology, 4th. edn.* San Francisco, California, United States of America: Benjamin Cummings, 2011.

Stanford Reseach Systems. "About lock-in amplifiers." 2015.

Sun, Y. and Scouten, C., "Method and apparatus for measuring electrical properties of cells," united States Patent Application.

Thompson, R. E., Lindau, M., and Webb, W. W., "Robust, high-resolution, whole cell patch-clamp capacitance measurements using square wave stimulation," *Biophysical Journal*, vol. 81, pp. 937–948, August 2001.